

Meteor generated plasma columns in E-region ionosphere: fields and diffusion

Y. S. Dimant* and M. M. Oppenheim†

Boston University

(Dated: March 29, 2017)

A meteoroid penetrating the Earth's atmosphere leaves behind a trail of dense plasma in the E-region ionosphere, a region where electrons are strongly magnetized while ions are demagnetized due to their frequent collisions with neutrals. While radar measurements of meteor trail evolution have been collected and used to infer meteor and atmospheric properties since the 1950s, no accurate quantitative model of trail fields and diffusion exists. This paper describes a theory and simulations of trail plasma physics which applies to the majority of small meteors. Unlike earlier papers, our theory assumes a significant angle between the geomagnetic field and the plasma trail and includes the important interaction between the trail and the background ionospheric plasma. This study provides quantitative knowledge of the spatial distribution and dynamics of the plasma density and electric field. This should enable meteor and atmospheric researchers to more accurately interpret radar observations of specular and non-specular meteor echoes.

I. INTRODUCTION

Meteoroids impacting the Earth's upper atmosphere have a number of important consequences by: depositing material, most notably metals and dust; damaging spacecraft; creating layers of material which radars and ionosondes detect; modifying the plasma density and conductivity of the lower ionosphere; leaving plasma columns which can be used for meteor burst communication and to monitor atmospheric conditions in the lower thermosphere. While large meteoroids generate spectacular optical displays, particles much smaller than a sand grain comprise the majority of all meteoroids and represent the major source of all extra-terrestrial material deposited in the Earth's atmosphere [1, 2]. Such small meteoroids can rarely be observed by a naked eye or even by a sensitive optical technique, but radars can easily detect them. Such observations become possible because meteoroids frequently enter the Earth's atmosphere with a sufficient speed (11–72 km/s) and energy to cause the formation of a dense plasma visible to radars. The front edge of this plasma can often be observed by high-power large-aperture (HPLA) radars, while smaller, lower-power radars can detect the residual trail as either specular or non-specular echoes.

Specular echoes, usually observed by small-aperture and HF-VHF radars, originate from parts of the plasma trail where the wavevector of the backscattered wave is nearly perpendicular to the axis of a slowly diffusing, quasi-cylindrical plasma trail (for review, see [2]). Non-specular meteor echoes observed by HPLA VHF or UHF radars like the one shown in Fig. 1 originate from trails where the specular condition is not necessarily satisfied but where the radar typically points close to perpendicular to the geomagnetic field [3, 4, 5, 6]. Non-specular echoes appear to result from small-scale electron density irregularities caused by plasma turbulence and measured when the radar wavevector lies parallel to the irregularity wavevector but with a wavenumber twice the irregularity wavenumber, satisfying the Bragg condition. A polar-

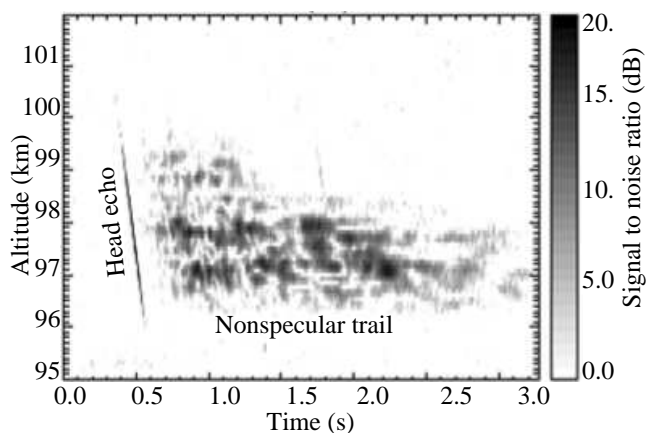


FIG. 1: Non-specular radar echo (Jicamarca Radio Observatory near the magnetic equator, July 12, 2005, 3:43 AM local time).

ization electric field, resulting from the plasma trail ambipolar diffusion, drives field-aligned instabilities which generate these irregularities [7, 8].

Modeling specular echoes requires knowledge of the spatial and temporal distribution of the plasma trail density, while modeling non-specular trails also requires knowledge of the evolution and structure of the polarization electric field which drives the instabilities. In a series of papers [8, 9, 10, 11, 12], Oppenheim, Dyrud and others have simulated the development of plasma instabilities in the meteor trail under conditions when the axis of an axially-symmetric cylindrical plasma trail was perfectly aligned with the geomagnetic field [or, in a two-dimensional (2D) case, making the trail a slab instead of a cylinder]. This is, however, a degenerate case because most of meteor trails are oriented at a significant angle with respect to the magnetic field. In the general case, electrons have anisotropic responses to the electric field, which significantly complicates theoretical description of the dense plasma trail evolution.

A number of studies have looked at the evolution of a dense plasma column in a collisional magnetized plasma. The earliest simulations [14, 15, 16] had restricted box sizes which could not properly describe the actual ionospheric situation.

*Electronic address: dimant@bu.edu

†Electronic address: meerso@bu.edu

Furthermore, numerical simulations alone cannot provide the parameter dependence of the plasma density and polarization electric field, which is of importance for modeling plasma instabilities. At the same time, analytical theory, even an approximate one, could provide such dependencies and would be an indispensable tool for the accurate interpretation of radar observations, meteoric and ionospheric diagnostics.

The analytical theory by Jones [17] represents a significant step forward. He proposed a 2D self-similar solution (SSS) of the meteor trail evolution, starting from an initial line density. Using a combination of a Gaussian spatial distribution of the plasma density with a parabolic distribution of the electric potential, Jones developed a mathematical scheme, which describes the initial evolution and structure of the trail plasma density reasonably well. However, it improperly describes the spatial structure of the polarization electric field because the assumed plasma density structure requires that the field goes to infinity with distance from the trail axis. As we show in this paper, that theory also fails to predict significant deviations from the self-similar diffusion at a later stage of the meteor trail evolution. The reason for this is that the SSS does not account for interaction with the background ionospheric plasma.

In the earlier stage of plasma trail diffusion, the background plasma density is usually small compared to the plasma density within the trail. However, this low-density plasma plays a crucial role for carrying electric currents originating from the trail during its ambipolar diffusion. This current significantly affects the evolution and structure of the trail density in the later stage. Further, the electrodynamic interaction of the meteor trail with the background ionosphere provides a natural restriction for the polarization electric field which drives plasma instabilities. The research presented in this paper includes the interaction of the trail with the background ionosphere.

Note that in a recent theoretical paper on meteor trail diffusion, Robson [18] (see also [19]) attempted to revise the previous theories. Robson's approach, however, seems invalid because, in addition to the quasineutral assumption, Robson assumed that the electron and ion fluxes along the magnetic field are equal. In the general case, the latter assumption causes the resulting electric field to have a significant non-zero curl. Estimates show, however, that the contribution of the induction electric field to the trail dynamics in the E region is negligible, so that to high accuracy the electric field within and around the trail should be electrostatic, i.e., curl-free (see Sect. VIII).

In order to improve modeling of non-specular trails and enhance our knowledge of plasma column diffusion and fields, we revisit this problem. As in the majority of the previous studies, we restrict ourselves to plasma columns that remain homogeneous along their length and assume constant electron and ion temperatures. Homogeneity along the trail implies that diffusion occurs only in the plane perpendicular to the trail, though electron fluxes have all three vector components. We further assume that the trail axis is directed at a sufficient angle to the geomagnetic field (in this paper, we restrict the analytical treatment to the purely orthogonal case). The paper differs from Jones [17] in that it includes the important effect

of the background ionospheric plasma. Finally, we consider only the case when there is no external electric fields or strong neutral winds which often exist in real E-region ionosphere, especially at high latitudes and in the equatorial region. We will describe these important effects in future papers. In this paper, we present results of both numerical simulations and analytical theory. The main result of this work is a quantitative description of meteor trail evolution and the polarization electric field associated with its ambipolar diffusion. Results of our analytical model and simulations agree remarkably well. We expect that applying our theoretical model to radar echoes from trails should help researchers obtain useful information about meteoroids and the surrounding atmosphere.

The paper is organized as follows. In Section II, we discuss qualitatively the ambipolar diffusion of meteor trails in the E-region ionosphere, introduce the concept of the residual potential and discuss some restrictions. In Section III, we present the equations for meteor fields and diffusion based on a simple two-fluid model of a highly collisional isothermal plasma and formulate proper boundary conditions. In Section IV we discuss results of our 2D finite-element simulations, which give us useful insights into finding the proper approach for the analytical treatment of the problem. In Section V, we present our analytical theory for the specific case of mutually orthogonal meteor trail axis and the geomagnetic field. In Section VI, we summarize our analytical results. In Section VII, we compare our theory with simulations quantitatively. In Section VIII, we discuss some caveats and implications of our theory. In Section IX, we give a summary of the paper. Appendices A to F give mathematical details of our analytical theory.

II. QUALITATIVE DESCRIPTION OF METEOR TRAIL DIFFUSION

In this section, we discuss qualitative aspects of the meteor trail diffusion which will allow us to formulate the problem and make appropriate simplifications.

A. Plasma physics conditions in E-region ionosphere

The majority of specular and non-specular radar echoes are observed in the lower E region at altitudes 90–120 km, where the neutral atmosphere is many orders of magnitudes denser than the ionospheric plasma. While the plasma left behind a fast meteoroid in the form of a diffusing trail can be several orders of magnitude denser than the background ionospheric plasma, it is usually much less dense than the neutral atmosphere. The neutral atmosphere remains essentially undisturbed by the plasma trail formation.

All characteristic spatial scales of the diffusion state are much larger than the Debye length. The typical diffusion time scale is much longer than the electron plasma period. Due to these, the quasi-neutrality holds to good accuracy, $N_e \approx N_i \equiv N$, where $N_{e,i}$ are the electron and ion densities, respectively.

In the lower E region, the charged particles collide predominantly with neutral particles rather than between themselves. The following inequalities hold: $\Omega_i \ll \nu_{in}$ and $\nu_{en} \ll \Omega_e$, where $\Omega_{e,i} = eB_0/m_{e,i}$ are the electron and ion gyrofrequencies; ν_{en} and ν_{in} are the electron-neutral and ion-neutral collision frequencies respectively; e is the elementary charge, $m_{e,i}$ are the electron and ion masses, respectively, and $B_0 = |\mathbf{B}_0|$ where \mathbf{B}_0 is the geomagnetic flux density. The above inequalities express the fact that electrons are strongly magnetized, while ions are demagnetized due to frequent collisions with neutrals. In the equatorial region, $B_0 \simeq 0.25 \times 10^{-4}\text{T}$, while at mid- and high latitudes $B_0 \simeq 0.5 \times 10^{-4}\text{T}$. In the E-region ionosphere, O_2^+ and NO^+ ions dominate: $m_i \simeq 30 m_p$, where m_p is the proton mass, so that $m_i/m_e \simeq 5.5 \times 10^4$. Throughout the E region, $\nu_{en} \simeq 10 \nu_{in}$.

Under conditions $\Omega_i \ll \nu_{in}$ and $\nu_{en} \ll \Omega_e$, the electron and ion diffusion responses to the external electric field differ significantly. The response of unmagnetized ions is nearly isotropic, while the responses of strongly magnetized electrons differ dramatically in the directions parallel and perpendicular to the magnetic field. The ion isotropic mobility g_i (defined via $\mathbf{V}_i = g_i \mathbf{F}/e$, where \mathbf{F} is the external force) is given by $g_i \approx e/(m_i \nu_{in})$. The corresponding electron mobilities represent tensor components determined via similarly defined relations between the electron velocity \mathbf{V}_e and the external force \mathbf{F} . In the diffusion approximation, the electron velocity \mathbf{V}_e is determined by the inertialess fluid momentum equation (in the neutral atmosphere frame of reference),

$$0 = -e(\mathbf{E} + \mathbf{V}_e \times \mathbf{B}_0) - \frac{\nabla P_e}{N} - m_e \nu_{en} \mathbf{V}_e, \quad (1)$$

where \mathbf{E} is the electric field, $P_e \approx NT_e$ is the electron pressure, and T_e is the electron temperature (in energy units) assumed constant. The mobility of magnetized electrons along the magnetic field is $g_{e\parallel} \approx e/(m_e \nu_{en})$, while in the perpendicular direction the electron mobilities are $g_{e\perp}^{\text{Hall}} = e/(m_e \Omega_e) = 1/B$ (the Hall mobility), and $g_{e\perp}^{\text{Ped}} \approx e \nu_{en}/(m_e \Omega_e^2)$ (the Pedersen mobility). While the parallel and Pedersen velocities, $\mathbf{V}_{e\parallel}$ and $\mathbf{V}_{e\perp}$, have the same directions as the corresponding components of the electric field, the Hall velocity, i.e., the $\mathbf{E} \times \mathbf{B}_0$ drift, is perpendicular to \mathbf{E} .

B. Ambipolar diffusion of plasma columns

At the earliest stage of trail plasma formation, kinetic processes associated with ionization of ablated material dominate. After a short time, however, the newly formed plasma cools down, typical transport velocities become much smaller than the ion-acoustic speed, and the trail spreads over distances at least several times the characteristic mean free path [20]. This can be considered as the beginning of the diffusion stage. In this paper, we restrict our treatment to this stage.

The meteoroid velocity is usually much higher than typical diffusion velocities. This means that the trail diffusion starts roughly simultaneously over a sufficiently long distance along the trail. Considering a part of the trail which is smaller than

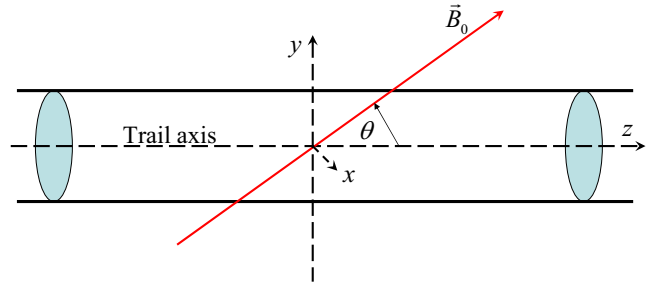


FIG. 2: Geometry of the trail and magnetic field.

the typical variation scale of ionospheric and neutral atmospheric parameters, we will neglect the spatial inhomogeneity and assume approximate translational symmetry along the trail axis, making all variations occur in the plane perpendicular to this axis.

Assuming a non-zero angle between the trail axis and the magnetic field, we will consider the diffusion of a 2D plasma trail with the following geometry, see Fig. 2. The trail density depends on the x and y coordinates, while it is invariant along the z coordinate. The homogeneous magnetic field \mathbf{B}_0 lies in the y, z plane. In this geometry, the plasma density gradient ∇N and the polarization electric field $\mathbf{E} = -\nabla\Phi$, where Φ is the electric potential, have only x and y components, while the electron drift velocity may have all three vector components.

In the special case when the trail axis is strictly parallel to \mathbf{B}_0 [9], the ambipolar diffusion is axially symmetric around the z -axis and its rate, determined by the ratio between the ion and electron Pedersen mobilities, roughly follows the lowest mobility. The collision frequencies of both electrons and ions are proportional to the neutral density which exponentially decreases with increasing altitude. The ratio of the electron Pedersen mobility to the isotropic ion mobility is given by the parameter

$$\psi \equiv \frac{g_{e\perp}^{\text{Ped}}}{g_i} = \frac{\nu_{en} \nu_{in}}{\Omega_e \Omega_i}. \quad (2)$$

At higher altitudes (usually above 97 km at the equatorial region and above 94 km at high latitudes) where the parameter ψ is less than unity, the lowest is the electron Pedersen mobility, so that the trail diffusion is determined by the slightly increased electron Pedersen diffusion rate. At lower altitudes where $\psi > 1$, the lowest is the ion mobility, so that the trail diffusion is determined by the slightly increased ion diffusion rate.

In the general case, the ambipolar diffusion is more complicated because all components of the polarization electric field are determined by the same scalar potential, Φ . This means that the diffusion in one direction necessarily affects the diffusion in other directions. Quasineutrality requires the divergences of the electron and ion fluxes to be equal, while the fluxes themselves may differ. Nevertheless, vector components of the electron and ion fluxes in any direction usually remain comparable. For 2D trail diffusion, if the angle between the magnetic field and the trail axis is not too

small (see the conditions in Sect. II C), there is a significant component of the electron pressure gradient along the magnetic field. Accordingly, there should be a significant component of the polarization electric field in this direction, $E_{\parallel} = -\nabla_{\parallel}\Phi$. The electron mobility along the magnetic field \mathbf{B}_0 (the ‘parallel’ mobility) is high, while the electron mobilities in the directions perpendicular to \mathbf{B}_0 are much lower. The electron parallel mobility is much greater than that of ions, $g_{e\parallel}/g_i \approx m_i\nu_{in}/m_e\nu_{en} \simeq 5500$ (Sect. II A). Because the average fluid velocity of the highly mobile electrons should be comparable to that of the low-mobile ions, according to Eq. (1), the parallel component of the polarization electric field should nearly cancel the electron pressure gradient,

$$e\nabla_{\parallel}\Phi \approx \frac{\nabla_{\parallel}P_e}{N} = T_e\nabla_{\parallel}\ln n, \quad (3)$$

where $n(x, y) = N/N_0$ and N_0 is the undisturbed ionospheric background density assumed constant and uniform. For isothermal electrons, the electric field and pressure can be combined into one force $(T_e + T_i)\nabla\phi_{\text{res}}$, where ϕ_{res} is a dimensionless ‘residual’ electric potential defined as

$$\phi_{\text{res}} \equiv \frac{e\Phi - T_e \ln n}{T_e + T_i}. \quad (4)$$

Because in our geometry the magnetic field direction has a finite y component, while the trail and fields are homogeneous along z , Eqs. (3) and (4) show that the residual potential within and around the trail is essentially independent of the y coordinate,

$$\phi_{\text{res}}(x, y) \approx \phi_{\text{res}}^0(x). \quad (5)$$

The concept of the residual potential ϕ_{res} is crucial for our numerical and analytical treatment. Furthermore, the macroscopic force that drives plasma instabilities is the total force acting on electrons, which is just proportional to the gradient of ϕ_{res} .

C. Restrictions on orientation of trail with \mathbf{B}

The effective cancelation of the electron pressure along the magnetic field described by Eq. (3) should only occur if the angle between the meteor trail axis and the magnetic field θ is high enough,

$$\theta \gg \Theta_0 \equiv \left(\frac{g_i}{g_{e\parallel}}\right)^{1/2} = \left(\frac{m_e\nu_{en}}{m_i\nu_{in}}\right)^{1/2} \simeq 1.35 \times 10^{-2}, \quad (6)$$

where the critical angle in degrees is $\Theta_0 \simeq 0.8^\circ$. This means that there is a significant component of the electric field along \mathbf{B}_0 to move electrons. The opposite limiting case of $\theta \ll \Theta_0$ corresponds to the diffusion at nearly perfect alignment between the trail axis and magnetic field when no parallel electron transport exists [10]. However the latter case, as well as the most difficult for analysis intermediate case, $\theta \sim \Theta_0$, are degenerate cases because of rather small value of the critical angle Θ_0 . It is evident that the overwhelming majority

of meteors penetrating the Earth’s atmosphere satisfy the condition given by Eq. (6). We will also require that the electron Pedersen velocity component along the y remains much smaller than the corresponding parallel velocity component. This yields the condition

$$\theta \gg \left(\frac{g_{e\perp}^{\text{Ped}}}{g_{e\parallel}}\right)^{1/2} = \frac{\nu_{en}}{\Omega_e} = \Theta_0\sqrt{\psi}, \quad (7a)$$

where the altitude dependent parameter ψ was defined in Eq. (2). For further simplicity, we will also require

$$\theta \gg \frac{\Omega_i}{\nu_{in}} = \frac{\Theta_0}{\sqrt{\psi}}. \quad (7b)$$

The parameter ψ decreases exponentially with increasing altitude, see, e.g., Fig. 2 in Ref. [21]. At the altitude range where electrons are magnetized while ions are unmagnetized, roughly between 80 and 120 km, the parameter ψ varies between 10^{-3} and 10^4 , so that restrictions given by Eqs. (7a) and (7b) combined are stronger than (6). In our major analytical treatment and simulations, we will discuss the particular case of $\theta = 90^\circ$, but in Appendix A, to find explicit expressions for the self-similar solution, we will consider a more general case restricted only by Eq. (7).

III. DIFFUSION EQUATIONS

If there is no significant ionization and recombination during the diffusion stage, then the line plasma trail density along the z axis remains nearly constant. The diffusion stage is adequately described by fluid equations which include two inertialess momentum equations for electrons and ions and two continuity equations. The quasineutrality condition makes the Poisson equation for the electric potential unnecessary. This set of equations can be readily reduced to two coupled nonlinear partial differential equations (PDEs) for the common plasma density and the electric potential,

$$\partial_t n + \nabla \cdot \mathbf{\Gamma}_i = 0, \quad (8a)$$

$$\nabla \cdot \mathbf{\Gamma}_i - \nabla \cdot \mathbf{\Gamma}_e = 0, \quad (8b)$$

where for unmagnetized ions and strongly magnetized electrons the diffusion flux densities, $\mathbf{\Gamma}_{e,i}$, are given by

$$\mathbf{\Gamma}_i = -n \frac{\nabla(e\Phi + T_i \ln n)}{m_i\nu_{in}}, \quad (9a)$$

$$\mathbf{\Gamma}_{e\parallel} = n \frac{\nabla_{\parallel}(e\Phi - T_e \ln n)}{m_e\nu_{en}}, \quad (9b)$$

$$\mathbf{\Gamma}_{e\perp} = n \left[\frac{\nu_{en}\nabla_{\perp}(e\Phi - T_e \ln n)}{m_e\Omega_e^2} + \frac{\hat{b} \times \nabla_{\perp}(e\Phi - T_e \ln n)}{m_e\Omega_e} \right]. \quad (9c)$$

Here the subscripts \parallel and \perp pertain to the directions parallel and perpendicular to the magnetic field \mathbf{B}_0 , respectively, and \hat{b} is the unit vector in the \mathbf{B}_0 direction. The first term in the

right-hand side (RHS) of Eq. (9c) describes the electron Pedersen flux, while the second term describes the electron Hall flux. Here we assume the isothermal approximation which is justified by frequent collisions with the huge thermal reservoir of neutral atmosphere (in a more general adiabatic process, we would have additional factors $\gamma_{e,i}$ in front of $T_{e,i} \ln n$).

Passing from Φ to the residual potential, Eq. (5), we rewrite Eqs. (8) in the x, y coordinates as

$$\partial_t n - D [\nabla^2 n + \nabla \cdot (n \nabla \phi_{\text{res}})] = 0, \quad (10a)$$

$$(1 + \psi) \partial_x (n \partial_x \phi_{\text{res}}) + Q \partial_y (n \partial_y \phi_{\text{res}}) + \mu (\partial_x \phi_{\text{res}} \partial_y n - \partial_x n \partial_y \phi_{\text{res}}) + \nabla^2 n = 0, \quad (10b)$$

where we introduced the ambipolar diffusion coefficient,

$$D \equiv \frac{T_e + T_i}{m_i \nu_{in}} = \frac{(T_e + T_i) \Theta_0}{e B_0 \sqrt{\psi}}, \quad (11)$$

a large dimensionless parameter

$$Q \equiv \frac{\sin^2 \theta}{\Theta_0^2} = \left(\frac{m_i \nu_{in}}{m_e \nu_{en}} \right) \sin^2 \theta \gg 1, \psi, \frac{1}{\psi}, \quad (12)$$

and a dimensionless Hall parameter

$$\mu = \frac{\nu_{in} \cos \theta}{\Omega_i} = \frac{\sqrt{\psi}}{\Theta_0} \cos \theta. \quad (13)$$

Here we used the definitions of ψ , Eq. (2), and Θ_0 in radians, Eq. (6). We also used Eq. (7a) and neglected small additions to the large parameter Q , which are associated with the ion and electron Pedersen mobilities along y .

For the analytical treatment, it is convenient to rewrite Eq. (10) in self-similar variables,

$$\xi = \frac{x}{(Dt)^{1/2}}, \quad \zeta = \frac{y}{(Dt)^{1/2}}. \quad (14)$$

As a result, we arrive at the following equations for $n(\xi, \zeta, t)$ and $\phi_{\text{res}}(\xi, \zeta, t)$:

$$t \partial_t n - \frac{\xi \partial_\xi n + \zeta \partial_\zeta n}{2} - \nabla^2 n - \nabla \cdot (n \nabla \phi_{\text{res}}) = 0, \quad (15a)$$

$$(1 + \psi) \partial_\xi (n \partial_\xi \phi_{\text{res}}) + Q \partial_\zeta (n \partial_\zeta \phi_{\text{res}}) + \mu (\partial_\xi \phi_{\text{res}} \partial_\zeta n - \partial_\xi n \partial_\zeta \phi_{\text{res}}) + \nabla^2 n = 0, \quad (15b)$$

where the new ∇ operator pertains to the variables defined by Eq. (14), $\nabla = (\partial_\xi, \partial_\zeta)$. Our solution of meteor trail diffusion applies this set of coupled PDEs for ϕ_{res} and n . Given homogeneous background plasma, neutral atmosphere, and magnetic field, we assume the following asymptotic boundary conditions,

$$n \rightarrow 1 \quad \text{and} \quad \phi_{\text{res}} \rightarrow 0 \quad \text{as} \quad x, y \rightarrow \pm \infty. \quad (16)$$

We also note that our problem has the following symmetry,

$$n(x, y) = n(-x, -y), \quad (17a)$$

$$\phi_{\text{res}}(x, y) = \phi_{\text{res}}(-x, -y). \quad (17b)$$

The following section describes a numerical solution of these equations and the next section describes their analytic solution.

IV. SIMULATIONS OF TRAIL DIFFUSION AND FIELDS

In this section, we discuss results of our numerical solution of Eq. (10) using a finite-element PDE solver FlexPDE [31]. The challenge of these simulations is to simultaneously resolve both the relatively small scale of the trail density variations and the large scale of the residual potential variations parallel to the magnetic field (along y). This requires the box size along x to be at least several times the effective trail size in that direction, σ_x , while the box size along y should be several times Θ_0^{-1} , i.e., more than two orders of magnitude, larger than the box size along x . FlexPDE uses an adaptive finite elements mesh in regions with high gradients to resolve the fields and densities with high precision, while uses a coarse mesh in regions where gradients remain small.

We tested the effects of a finite simulation box on the solution by varying its size. We also varied boundary conditions, setting either the density disturbances, $\Delta n(t) \equiv n(t) - 1$, and ϕ_{res} , or the corresponding flux densities, Eq. (9), to zero on the boundaries. These tests demonstrated that, for sufficiently large box sizes, the solution in the inner region remained essentially unaffected by the choice of boundary conditions.

In numerical simulations, as well as in the analytical theory (Sect. V), we have explored the strictly perpendicular case of $\theta = 90^\circ$ ($\mu = 0$). In this case, we solved Eq. (10) with $Q = 5500$ corresponding to $m_i/m_e = 5.5 \times 10^5$ and $\nu_{en}/\nu_{in} = 10$, see Sect. II A. As the initial condition at time $t = t_0$, we chose a narrow and dense column of plasma, described by the self-similar solution (SSS). We used normalized units where the diffusion coefficient $D = 1$ and the initial time for the SSS solution $t_0 = 1$, so that the initial spatial distribution of the total normalized plasma density $n = N/N_0$ was given by

$$n(x, y, 1) = 1 + \Delta n_0 \exp \left[-\frac{(1 + \psi)x^2}{4\psi} - \frac{y^2}{4} \right]. \quad (18)$$

The characteristic sizes of the initial Gaussian density distribution of the trail in the x and y directions, $\sigma_{x0} = [2\psi/(1 + \psi)]^{1/2}$ and $\sigma_{y0} = \sqrt{2}$, are nearly equal for $\psi \gg 1$ (lower altitudes), but differ significantly for $\psi \ll 1$ (higher altitudes). To check the effect of the initial conditions, we tried different initial Gaussian density distributions corresponding to the same trail line density. We have found that, after the time needed for the trail to diffuse over a distance several times the original size of the trail, the solution becomes virtually the same. Hence, it is only weakly sensitive to the actual initial peak cross-section.

Equation (10b) involves no time derivatives, so that formally ϕ_{res} needs no initial condition. However, the FlexPDE application requires setting initial conditions for all variables. In our simulations, we usually set up $\phi_{\text{res}}(t_0) = 0$. We tested that after a rather short time, the solver automatically sets up a time-dependent spatial distribution of ϕ_{res} which proves to be independent of the initial condition for ϕ_{res} .

Bearing in mind the symmetry along the y direction (i.e., parallel to \mathbf{B}_0), we simulated a half of the entire space ($y \leq 0$) with boundary conditions at $y = 0$ given by zero derivatives of both n and ϕ_{res} . The box size, $|y|_{\text{max}} = 1000$, was always at least two orders of magnitude larger than $\sigma_y(t)$, but

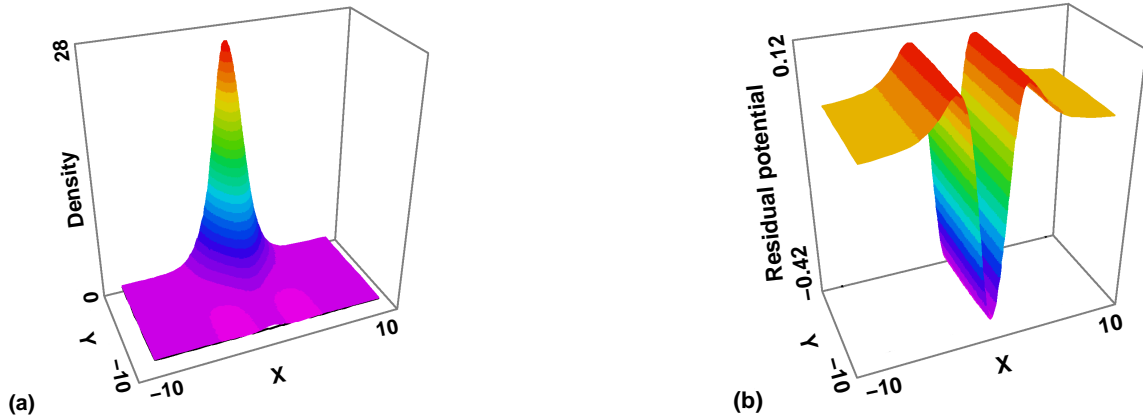


FIG. 3: Typical structure of plasma density (a) and residual potential (b). Here $\psi = 0.2$, $\Delta n_0 = 100$, and $t = 2.5$ (the background density corresponds to $n = 1$ and the initial time for the self-similar solution $t_0 = 1$).

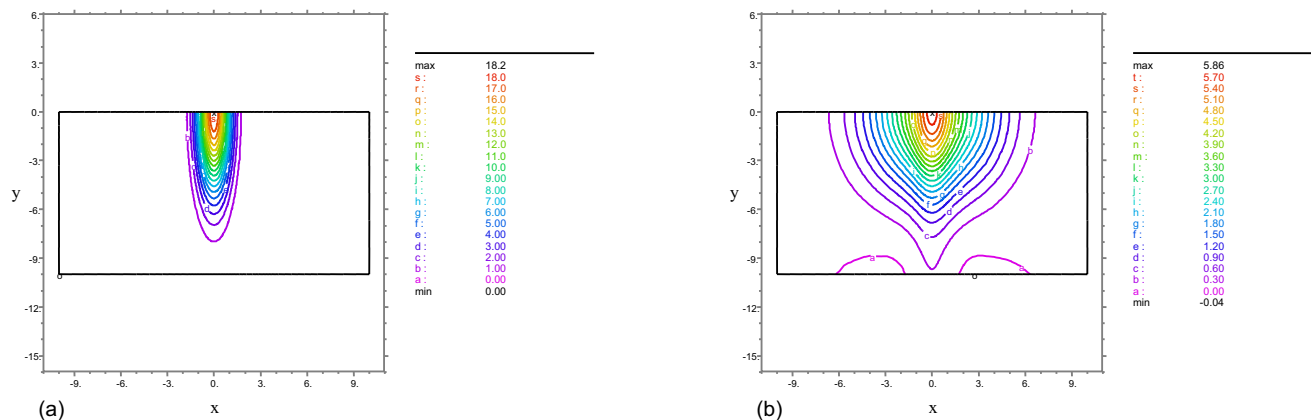


FIG. 4: Contours of trail density in the x, y -plane for $\psi = 0.05$, $\Delta n_0 = 100$, $t = 5.5$: (a): self-similar solution, (b): simulation.

we needed to keep it that long because of the long-extended residual potential.

In order to model different stages of trail diffusion we performed several overlapping runs by varying the initial peak densities from $\Delta n_0 = 10^4$ to $\Delta n_0 = 10$. We usually finished each run at $t = 40$, so that the box size $x_{\max} = 30$ remained at least several times $\sigma_x(t)$. Because of higher anisotropy and stronger gradients, the cases of small ψ are much more time and resource consuming than those of $\psi \gtrsim 1$. On a 3GHz Pentium 4 Windows-based PC, our runs lasted from several hours (for $\psi = 10$) to more than a week (for $\psi = 0.05$). Unfortunately, FlexPDE intrinsic restrictions have not allowed us to simulate $\psi < 0.05$.

To monitor the accuracy of simulations, we used general relations for the residual potential outlined in Appendix D and the exact property of density disturbance integrals (DDIs) which is analytically derived in Appendix E.

Figure 3 shows typical plasma density and residual potential plotted over the small fraction of the simulation box nearest the trail a short time after the simulation begins. Figure 4 compares an example of the trail density contours in the x, y -plane corresponding to the SSS (a) and to the full simulation (b) after the trail has diffused to several of its initial radius. Our simulations have revealed the following major features:

1. Initially, the plasma density distribution within the trail closely follows the anisotropic (for $\psi \lesssim 1$) SSS. At a later stage, as the peak density falls, the trail remains nearly Gaussian in each direction but becomes more isotropic than does the SSS, see Fig. 4, and it diffuses faster, with the isotropic ambipolar diffusion rate given described by Eq. (11). The transition from anisotropic to nearly isotropic diffusion usually takes place while the peak density remains much larger than

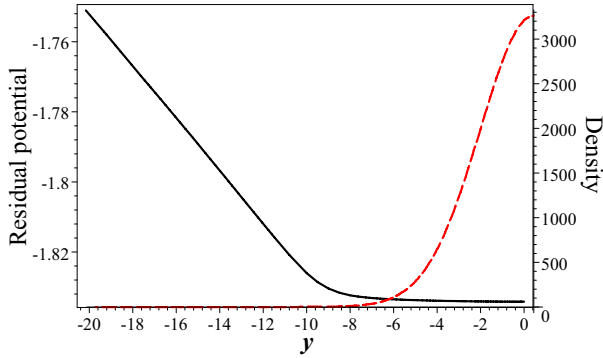


FIG. 5: Typical variation parallel to the magnetic field (along y) at $x = 0$ of residual potential (solid curve, left scale) and trail density (dashed curve, right scale) [for $\psi = 0.2$, $\Delta n_0 = 10^4$, $t = 3$]. In the near-trail region, the density has exponentially strong variation along y , while the residual potential varies only within several percent of its maximum absolute value. At some point beyond the trail (here about $u = -10$) the potential acquires a noticeable u -derivative (electric

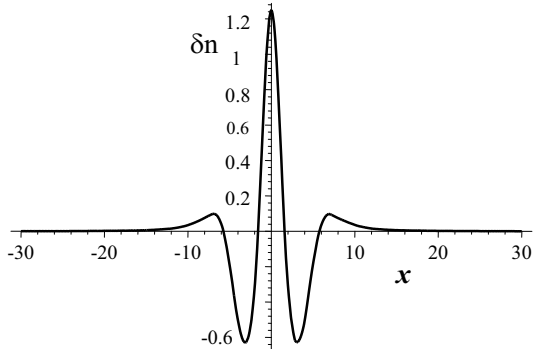


FIG. 6: Disturbances of background density beyond the trail perpendicular to the magnetic field (along x) [for $\psi = 0.2$, $\Delta n_0 = 10^4$, $t = 3.5$ at the coordinate $|y| = 20$ located well beyond the trail].

the background density. Section V discusses our analytical model for this point.

2. The residual electric potential spreads along y well beyond the trail, see Fig. 5, with spatial gradients along y much less than those along x . Along x it has a non-monotonic symmetric structure with a deep minimum at the trail center and two symmetric maxima around it, as shown in Fig. 3(b). At the later stage, when the trail diffusion becomes nearly isotropic (see Feature 1), the residual electric field becomes much smaller than that for the SSS.
3. Beyond the trail, where the exponentially small trail density is much less than the background density, the residual electric field extending along \mathbf{B}_0 may substan-

tially disturb the density as shown in Fig. 6. The field evacuates plasma from the region that maps along \mathbf{B}_0 the potential minimum back to those about the potential maxima. As a result, the perturbation density evolves in antiphase to the potential distribution along with a maximum at $x = 0$ and two symmetric minima roughly at x where the residual potential has the two maxima, as visible on the edge of Fig. 3(a). In our simulations, the maximum central density compression more than doubled the undisturbed background density, while the depletions reached about 80% of that. These strong disturbances were reached near the trail when the peak trail density was at least several orders of magnitude larger than the background density, see Fig. 6. In all other cases or locations, relative density disturbances were small. We estimate them in Sect. V D.

We will discuss these features in Sects. V and VII, when describing our analytical theory and comparing it with simulations. Here we only give brief explanations to some features.

Feature 1: At the later stage of trail diffusion, when the initially dense trail density becomes much less dense (but remains much denser than the background plasma), its gradual isotropization and acceleration of diffusion to the ambipolar isotropic rate are due to the sharp decrease with time in the residual electric field (Feature 2). In this case, the total force acting on electrons becomes so small that diffusion is mainly determined by the total pressure gradient acting on ions and, hence, is virtually unaffected by the external magnetic field. The significant reduction of the residual electric field is due to the response of the background plasma which is not included in the SSS. To provide quasineutrality, a less dense trail starts attracting more charged particles from the background, thus reducing the need for strong ambipolar electric field.

Feature 2: The extension of the residual potential along y , i.e., parallel to the external magnetic field \mathbf{B}_0 , is due to the high electron mobility along \mathbf{B}_0 . The deep potential minimum in the trail center is formed by anisotropic ambipolar trail diffusion. These two factors are included in the SSS and are independent of the existence of background plasma. However, the two maxima seen in the residual potential distribution along x , see Fig. 3(b), are due to background plasma. The electron and ion fluxes originating in the trail extend into the background ionosphere with sharply anisotropic and quite different patterns, while the divergences of the two fluxes remain balanced. Beyond the trail, these patterns have a quadrupole-like structures providing current closure. To drive the return currents, the background ionosphere develops potential gradients which oppose those within the trail, i.e., those responsible for the trail diffusion. This gives rise to the two symmetric potential bumps around the deep potential minimum and draws background plasma into the trail edges.

The simulations allow us to determine diffusion rates and isotropy for a range of altitude-dependent ψ . This will be presented in conjunction with our analytical theory in Sect. VII.

V. ANALYTICAL THEORY

Here we discuss our analytical theory for the ‘perpendicular’ case of $\theta = 90^\circ$ ($\mu = 0$), when a double mirror symmetry,

$$n(\xi, \zeta) = n(\pm\xi, \pm\zeta), \quad (19a)$$

$$\phi_{\text{res}}(\xi, \zeta) = \phi_{\text{res}}(\pm\xi, \pm\zeta), \quad (19b)$$

takes place. The Hall velocity of electrons is directed strictly along the trail axis, so that it does not affect the 2D diffusion of the plasma trail. In the general case of $\theta \neq 90^\circ$, the Hall mobility breaks the double mirror symmetry but keeps a rotational (by 180°) symmetry around the trail axis, Eq. (17). For sufficiently large angles θ , distortions caused by the Hall mobility are relatively small (see Appendix A), so that the double mirror symmetry roughly takes place. However, the Hall mobility affects the aspect ratio of typical scales along each axis. We reserve the more general case for future work.

The trail diffusion and evolution of the ambipolar fields are described by two coupled nonlinear PDEs for the plasma density and the residual potential, see Eqs. (10) or (15). Our theory provides an approximate analytical solution of both inter-related problems. The key point of the theory has been the inclusion of the background plasma into consideration. In so doing, even for $\mu = 0$, one cannot find the exact analytical solution of the coupled equations. However, based on the existence of the large parameter $Q = \Theta_0^{-2} \simeq 5500$, Eq. (12), and on the insight from our simulations, see Sect. IV, we have developed an approximate approach based on the perturbation technique.

We have used the fact that the initially narrow and dense trail keeps nearly Gaussian density distribution during the trail lifetime even if the diffusion rate is changing with time, see Sect. IV. Given the characteristic scale of the Gaussian distribution, we have reduced Eq. (15b) to a simpler equation for the residual potential. This one-dimensional (1D) linear integrodifferential equation is the governing equation of our theory. It has two equivalent forms that depend upon only one dimensionless parameter ρ . This master parameter is proportional to the square of the characteristic Gaussian scale along x , $\rho \propto \sigma_x^2(t)$, see Eq. (65) below, and, hence, monotonically grows with time. Approximate solutions of the governing equation in different domains of $\rho(t)$ have allowed us to obtain the spatial distribution of the residual electric potential in the entire 2D space.

The trail diffusion is mainly determined by the parabolic behavior of the potential along x within the central region and is practically insensitive to the potential behavior outside this region. This has allowed us to find from Eq. (15a) the explicit time dependence of $\rho(t)$ and thus close the solution. As a result, we have obtained approximate analytic expressions describing the trail diffusion and the evolution of the residual electric fields. These expressions reasonably well agree with the numerical results and can be used for quantitative predictions.

Our analytical theory consists of several major steps: (1) obtaining explicit expressions for the self-similar solution; (2)

solving an equation for the electric potential in the ‘far zone’ where the density disturbances are relatively small; (3) obtaining the governing equation for the residual potential in the ‘near zone’ depending on the master parameter ρ ; (4) solution of this equation in different ranges of ρ ; (5) finding expressions for $\rho(t)$ in the initial value problem, which gives the approximate solution of the trail diffusion problem and closes the solution for the residual potential; (6) estimating density disturbances of the background plasma beyond the trail and obtaining a correction factor for $\rho \gg 1$ at a later stage of trail diffusion. We have implemented steps (1) to (3) in Appendices A to C, while in Sect. V A we will only explain the basic ideas and discuss the resultant governing equation. We have implemented steps (4) to (6) in Sect. V B to V D.

A. Governing equation for near-zone residual potential

Here we briefly describe the governing equation intended for the solution of the residual potential problem. Given the trail density spatial distribution, this approximate equation is derived from Eq. (15b). The derivation requires separation of the entire ξ, ζ plane into two overlapping regions: the near zone,

$$|\zeta| \equiv \frac{|y|}{(Dt)^{1/2}} \ll Q^{1/2}, \quad (20)$$

and the far zone,

$$|\zeta| \gg 1. \quad (21)$$

We emphasize that the terms ‘near’ and ‘far’ pertain to the coordinate ζ only, so that the near zone includes the entire ξ -axis (the x -axis). The residual potential in the near zone is ξ dependent but remains nearly constant in the ζ direction, i.e., along B_0 , see Eq. (5), making its calculation a 1D problem.

In the far zone, which includes the background ionosphere only, the residual potential has a slow ζ dependence, but we may roughly neglect there density disturbances (see Appendix B and Sect. V D). The fact that divergences of the electron and ion fluxes are nearly equal, as required by quasi-neutrality, results in the Laplace equation in terms of some renormalized coordinates. In those renormalized coordinates, the entire near zone reduces to a thin cut which provides boundary conditions for the Laplace equation in each of the two half-spaces, $\zeta > 0$ or $\zeta < 0$. Because of the symmetry, it is sufficient to consider only one of these half-spaces ($\zeta > 0$). Given the residual potential in the near zone ϕ_{res}^0 , a straightforward solution of the Laplace equation in integral form yields the spatial distribution of the residual potential in the entire 2D space, as described by Eq. (B4).

Using the Gaussian approximation of the trail plasma density, Eq. (C7),

$$n_{\text{Trail}} = \frac{\Delta n_0 t_0}{t} \sqrt{\frac{q_0}{q(t)}} \exp \left[-\frac{1}{4} \left(\frac{\xi^2}{q(t)} + \zeta^2 \right) \right], \quad (22)$$

and integrating it over the near zone, we obtain the sought-for boundary condition for the Laplace equation. This integration

involves ϕ_{res}^0 (with still unknown ξ dependence) multiplied by the corresponding trail density integral over the coordinate ζ . Associating the upper half-space with a complex plane in terms of renormalized coordinates and using analytical properties of the potential in the far zone (see Appendix B), in Appendix C we obtain for the the near-zone residual potential an integrodifferential equation in two different, but equivalent, forms:

$$\frac{2\rho}{\pi^{3/2}} e^{\frac{\eta^2}{4}} \mathcal{P} \int_{-\infty}^{\infty} \frac{\varphi(\tau)}{\tau - \eta} d\tau + \partial_{\eta} \varphi(\eta) = \eta, \quad (23a)$$

$$\rho \varphi(\eta) - \frac{1}{2\sqrt{\pi}} \mathcal{P} \int_{-\infty}^{\infty} \frac{\partial_{\tau} \varphi(\tau)}{\tau - \eta} e^{-\tau^2/4} d\tau = S(\eta). \quad (23b)$$

Here the renormalized near-zone residual potential φ and coordinate η are defined by

$$\varphi(\eta) = 2(1 + \psi) \phi_{\text{res}}^0(\xi), \quad (24a)$$

$$\eta = \frac{\xi}{q^{1/2}} = \frac{x}{(qDt)^{1/2}} = x \sqrt{\frac{\gamma}{\rho D}}. \quad (24b)$$

The coupled dimensionless parameters $q(t)$ and $\rho(t)$ are proportional to the square of the Gaussian peak dispersion with respect to x coordinate, σ_x^2 , Eq. (51b),

$$\rho(t) = \gamma q(t) t = \frac{\gamma \sigma_x^2}{2D} = \frac{\pi \sigma_x^2 N_0}{\sqrt{1 + \psi} \Theta_0 N_{\text{lin}}}, \quad (25)$$

where

$$\gamma = \frac{1}{2\Theta_0 \Delta n_0 t_0 \sqrt{\psi}} = \frac{2\pi N_0 (T_e + T_i)}{\sqrt{\psi} (1 + \psi) N_{\text{lin}}^z e B_0} \quad (26)$$

and N_{lin} is the line plasma density of the trail along its axis z .

The important function $S(\eta) = \eta e^{-\eta^2/4} \int_0^{\eta/2} e^{\tau^2} d\tau - 1$ in the RHS of Eq. (23b), see also Eq. (C17), together with the highest-order power-series approximations of $S(\eta)$, Eqs. (C20), (C21), is shown in Fig. 7. In Sect. VB, we will see that this function is a good qualitative, and in some cases even quantitative, representation of the residual potential in the near zone.

Equivalent Eqs. (23a,b) are linear integrodifferential equations in renormalized variables defined by Eq. (24). In these variables, these equations depend upon only one dimensionless parameter ρ . We will use one of two equivalent Eqs. (23a,b) depending upon the convenience for the specific analysis. In Section D, we discuss the general analytical properties of the solution, which can be used for monitoring the solution. In particular, under assumed approximations, the integral of $\phi_{\text{res}}^0(\xi)$ over ξ should be equal to zero. This explains mathematically the non-monotonic, two-bump structure of the residual potential in the near zone observed in our numerical calculations (see Sect. IV, Feature 2).

The physical sense of the outlined mathematical procedure is that different patterns of the electron and ion fluxes in the far

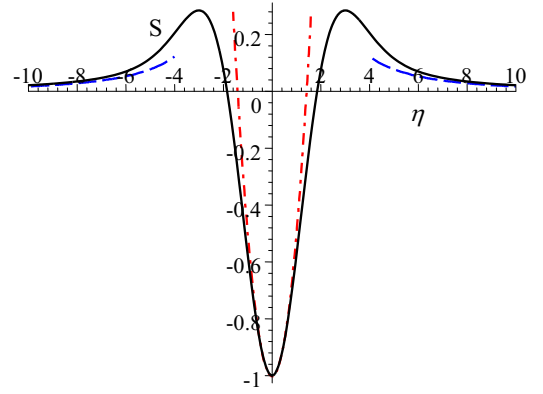


FIG. 7: Function $S(\eta) = \eta e^{-\eta^2/4} \int_0^{\eta/2} e^{\tau^2} d\tau - 1$, Eq. (C17) (solid curve), along with its parabolic approximation, $-1 + \eta^2/2$, Eq. (C20) (dash-dotted curve), and large- η asymptotics, $2/\eta^2$, Eq. (C21) (dashed curve).

zone create a feedback to the near zone. The non-monotonic structure of the residual potential (in each of the two half-spaces, $x > 0$ and $x < 0$), can be explained as follows. The total force acting on negatively charged electrons is proportional to $e \nabla \phi_{\text{res}}^0$. Within the major trail, this force via electron Pedersen diffusion pushes electrons outwards. This requires the residual potential to have a minimum in the trail center. Well beyond the trail, different electron and ion flux patterns form return fluxes in the background ionosphere. On approaching the trail, these fluxes are directed inwards which requires oppositely directed gradients of the residual potential. This gives rise to the two bumps of the residual potential.

B. Solution of governing equation

Having solved equations for the residual potential in the near zone and using formulas of Appendix B, we can find the ambipolar electric field and estimate the plasma density disturbances both in the trail and in the background ionosphere. Equivalent Eqs. (23a,b) have singular Cauchy kernels. While general methods for solving singular integral equations exist [22, 23], we are unaware of such methods for Cauchy-type integrodifferential equations. Even the existence and uniqueness of the solutions of such equations is not *a priori* known and should be studied individually for each specific equation. Nevertheless, for each value of ρ , Eq. (23) has the unique solution. We will not dwell here on the proof, but note that the uniqueness of the solution is provided by the positive sign of ρ [for negative ρ , Eq. (23) would have infinite number of solutions].

While the equation for $\varphi(\eta)$ has the unique solution, it is not possible to find it analytically in the general case. In this section, we discuss approximate solutions of Eq. (23) for various ranges of ρ . We will proceed from the simplest case to the more complicated ones.

1. Late stage diffusion, $\rho \gg 1$

The simplest limiting case of $\rho \gg 1$ corresponds to a sufficiently late stage of the meteor trail diffusion, when the peak trail density exceeds the background not too significantly, $(N_{\max} - N_0)/N_0 \ll \psi^{1/2}/[2(1 + \psi)\Theta_0]$ ($\psi^{1/2}/\Theta_0 = \nu_{in}/\Omega_i \gg 1$). In this limiting case, one can solve Eq. (23b) using a perturbation technique. For $\rho \gg 1$, the integral term in Eq. (23b) is small compared to the first term in the RHS. To the zeroth order, we can neglect the integral term so that the zero-order solution is given by $\varphi(\eta) \approx \varphi^{(0)}(\eta)$,

$$\varphi^{(0)}(\eta) = \frac{S(\eta)}{\rho}. \quad (27)$$

In the central region, $|\eta| \ll 1$, the renormalized amplitude of the electric field, $\partial_\eta \varphi \approx \eta^2/(2\rho)$, proves to be much less than that for the self-similar solution, $\partial_\eta \varphi^{SS} = \eta^2/2$.

The physical reason for much smaller residual electric field is as follows. When electrons leave a sufficiently dense trail, mainly along the magnetic field, slowly diffusing ions create a significant ambipolar electric field to retard electrons. If the trail is not dense then there are enough background electrons to substitute for those leaving the trail, so that no strong residual electric field is needed. The integral term in Eq. (23b), corresponding to the term $\partial_\eta \varphi$ in Eq. (23a), describes the electric field associated with the trail electrons, while the remaining terms in the left-hand sides (LHSs) include the effect of background electrons. In the case of $\rho \gg 1$, the latter terms dominate.

To verify that the neglected integral term is really small, we need to obtain the next-order approximation. To this end, we substitute the zeroth-order expression $\varphi^{(0)}(\eta)$ to the integral term in Eq. (23b). Using Eqs. (C22)–(C24), we obtain the first-order approximation,

$$\varphi^{(1)}(\eta) = \frac{S(\eta)}{\rho} - \frac{J(\eta)}{\rho^2} \approx \frac{S(\eta)}{\rho} - \frac{lS(p\eta)}{\rho^2}, \quad (28)$$

where $J(\eta)$ is given by Eq. (C23) and $l \approx 0.643$, $p \approx 1.546$, Eq. (C25). Figure 8 shows the function $J(\eta)$ and its approximate counterpart $\tilde{J}(\eta) = lS(p\eta)$. The two functions practically perfectly agree everywhere except the two symmetric maxima. While the approximate expression in the RHS of Eq. (28) is less accurate, it is much simpler for analysis. Equation (28) clearly shows that since the second term is small compared to the first one the perturbation approach employed here is consistent.

As seen from Eq. (28), for $\rho \gg 1$ the residual potential is approximately a linear combination of two S -functions with different arguments. The function $S(\eta)$ has major qualitative properties of the residual potential shown in Fig. 3(b). One can also check that this function automatically satisfies the general analytical properties of the solution given by Eqs. (D1), (D4), and (D7).

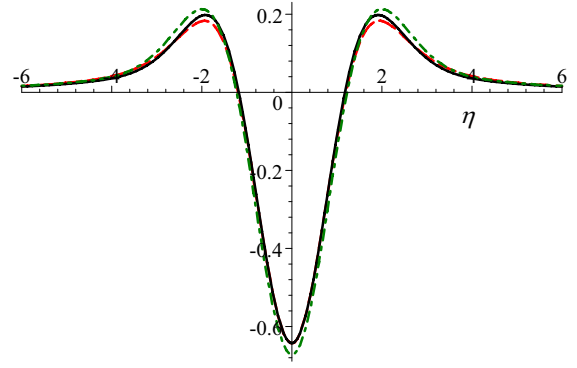


FIG. 8: First-order corrections in $\varphi^{(1)}(\eta)$, Eqs. (28) and (31), multiplied by $-\rho^2$. Solid curve: $J(\eta)$, Eq. (C23); dashed curve: $\tilde{J} = lS(p\eta)$, Eq. (C24); dot-dashed curve: the second term (multiplied by $-\rho^2$) in the RHS of Eq. (31) for $\rho \gg 1$.

2. Intermediate case, $\rho \sim 1$

The perturbation technique of the previous subsection fails for $\rho \sim 1$, and especially for $\rho \ll 1$. In these cases, we have found no rigorous analytical solution. However, we have developed an approximate approach for solving the integrodifferential equations using analytical fitting with iterations. This approach is similar to the numerical shooting method. Assuming a reasonable initial approximation for a zero-order iteration $\varphi(\eta) \simeq \varphi^{(0)}(\eta)$ with adjustable parameters, we may put this function into the integral term of one of the integrodifferential equations and find the next-order iteration. Comparison between the two iterations at the critical central region allows us to adjust the parameters in order to find the best fit.

The two forms of the integrodifferential equation for the near-zone potential, Eqs. (23a,b), are equivalent in rigorous mathematical sense, but this is not so if we seek the trial-and-error approximate solutions. For the intermediate case of $\rho \sim 1$, it is more convenient to use Eq. (23b). This allows us to disregard the correct asymptotic behavior, Eq. (D4), of the initial trial function [this behavior is required in Eq. (23a) to eliminate the diverging effect of the exponentially growing factor in front of the integral].

We start by choosing a simple trial function, $\varphi^{(0)}(\eta)$, which satisfies the condition (D1) but not necessarily (D4). Putting it into the integrodifferential term in Eq. (23b), we calculate the first-order iteration,

$$\varphi^{(1)}(\eta) = \frac{1}{\rho} \left(\frac{1}{2\sqrt{\pi}} \mathcal{P} \int_{-\infty}^{\infty} \frac{\partial_y \varphi^{(0)}(y)}{y - \eta} e^{-y^2/4} dy + S(\eta) \right). \quad (29)$$

It can be readily shown that $\varphi^{(1)}(\eta)$ will automatically satisfy Eqs. (D1) and (D4). In principle, the same procedure could be continued further to calculate next-order approximations $\varphi^{(2)}(\eta)$, $\varphi^{(3)}(\eta)$, but because of increasing complexity the analytical calculation of the integrals is hardly possible.

To make calculations simpler, we choose as the initial function $\varphi^{(0)}(\eta)$ the even η -derivative of the odd function

$$-A\eta \exp(-\lambda\eta^2),$$

$$\varphi^{(0)}(\eta) = A(2\lambda\eta^2 - 1) \exp(-\lambda\eta^2). \quad (30)$$

Because the generating function $-A\eta \exp(-\lambda\eta^2)$ tends to zero as $\eta \rightarrow \infty$, the trial function with $\phi(\eta) = \varphi^{(1)}(\eta)$ automatically satisfies Eq. (D1). Besides, in the central part it qualitatively looks like the expected residual potential around the major trail.

Now we find $\varphi^{(1)}(\eta)$, Eq. (29). Direct calculation yields

$$\begin{aligned} \varphi^{(1)}(\eta) &= \frac{S(\eta)}{\rho} - \frac{2\lambda A}{\rho\sqrt{1+4\lambda}} \\ &\times \left[\frac{4\lambda}{1+4\lambda} + (3-2\lambda\eta^2) S(\eta\sqrt{1+4\lambda}) \right]. \end{aligned} \quad (31)$$

The major residual potential is located in the central region, where it is nearly parabolic. It is natural then to fit the parabolic behavior of the two functions, $\varphi^{(0)}(0)$ and $\varphi^{(1)}$, at small $|\eta|$. For $\rho > 0.1$, this will provide a good fit in the entire central region and, due to Eq. (D1), a reasonable fit in the nearby region as well. Fitting the two parabolas,

$$\varphi^{(0)}(0) = \varphi^{(1)}(0), \quad \partial_{\eta\eta}^2 \varphi^{(0)}(0) = \partial_{\eta\eta}^2 \varphi^{(1)}(0), \quad (32)$$

we obtain two equations for the two unknown parameters, λ and A . Using the Taylor expansion for the function $S(\eta)$ at small η , Eq. (C20), and similar for $\varphi^{(0)}(\eta)$, Eq. (30), we obtain

$$\rho = \frac{8\lambda^2(5+16\lambda)}{(1-6\lambda)(1+4\lambda)^{3/2}}, \quad (33a)$$

$$A = \frac{(1-6\lambda)(1+4\lambda)^{3/2}}{2\lambda(3+10\lambda+16\lambda^2)}. \quad (33b)$$

These expressions give an implicit dependence of the two fitting parameters, A and λ , on ρ . The parameter λ varies in the range from 0 ($\rho \rightarrow 0$, $A \rightarrow \infty$) to $1/6$ ($\rho \rightarrow \infty$, $A \rightarrow 0$). We cannot explicitly express parameters A and λ in terms of ρ . However, we can determine the asymptotic behavior of $A(\rho)$ and $\lambda(\rho)$ at large and small values of ρ and construct interpolating formulas that would provide a reasonable approximation to the exact solution. We choose the following interpolation formulas,

$$\lambda \approx \lambda_{\text{int}}(\rho) = \left(\frac{\rho + c\rho^2}{40 + b\rho + d\rho^2} \right)^{1/2}, \quad (34a)$$

$$A \approx A_{\text{int}}(\rho) = \left(\frac{10 + N\rho}{9\rho + G\rho^2 + N\rho^3} \right)^{1/2}, \quad (34b)$$

where $b \approx 122.7$, $c \approx 1.52$, $d \approx 54.74$, $N \approx 14.67$, and $G \approx 29.7$. These approximations deviate from the exact functions $\lambda(\rho)$ and $A(\rho)$ only several percent at worst (when ρ is small).

For large ρ , the first-order solution $\varphi^{(1)}(\eta)$ matches the corresponding solution obtained in the previous subsection. Indeed, the major terms in Eqs. (28) and (31) are the same, $S(\eta)/\rho$. Furthermore, for $\rho \gg 1$ we have $\lambda \approx 1/6$ and

$A \approx 1/\rho$. In this case, the smaller second term in the RHS of Eq. (31) approximately agrees with the second term in Eq. (28) with the largest mismatch near the two maxima of $\varphi^{(1)}(\eta)$, $|\eta| \approx 2$. Figure 8 shows that the relative mismatch there is about 10% for exact $\varphi^{(1)}(\eta)$ in Eq. (28) and is roughly twice as large for the approximate expression [in terms of $S(p\eta)$]. In all other locations, the agreement is much better. Furthermore, because this is the mismatch between the two minor terms, the relative mismatch between the two full solutions $\varphi^{(1)}(\eta)$, Eqs. (28) and (31), is ρ times smaller.

Figure 9 shows the fitting solution for $\rho = 1$ and $\rho = 0.1$ and the parabolic SSS for the residual potential, $\varphi^{\text{SS}}(\eta) = \varphi(0) + \eta^2/2$. From Fig. 9(a) we see that for $\rho = 1$ the two approximations, $\varphi^{(0)}(\eta)$ and $\varphi^{(1)}(\eta)$, are reasonably close to each other in the entire central region, but the self-similar solution deviates significantly from both. Figure 9(b) shows that for small ρ the two approximations start deviating from each other even in the central region. The reason for this is that the lowest parabolic term $\propto \eta^2$ in the Taylor expansion for $\varphi^{(1)}(\eta)$ becomes so small that the higher-order terms $\propto \eta^4$ start playing the major role, even at sufficiently small η . At the same time, the first-order approximation $\varphi^{(1)}(\eta)$ closely approaches the self-similar solution in the central region, as is should for small ρ (see the following Section).

3. Early stage diffusion, $\rho \ll 1$

The limiting case of $\rho \ll 1$ deserves special attention because it usually applies when the meteor trail is first detected. This case corresponds to the early diffusion stage of a sufficiently dense plasma trail, when the trail density evolution follows the SSS, so that $q \approx q_0 = \psi/(1+\psi)$, see Eq. (50) below. According to Eqs. (25) and (26), if $\rho \ll 1$ then

$$n_{\text{max}} \equiv \frac{N_{\text{max}}}{N_0} \gg \frac{\psi^{1/2}}{2(1+\psi)\Theta_0} = \frac{\nu_{in}}{2(1+\psi)\Omega_i}.$$

This case is the most difficult case for the analysis. Being unable to obtain a rigorous solution in the entire range of $\varphi(\eta)$, we can construct a reasonable approximation. Qualitatively, the solution has the same basic form as for $\rho \gtrsim 1$, viz., a deep potential minimum surrounded by two symmetric maxima. Smallness of ρ suggests neglecting the integral term in the RHS of Eq. (23a), so that we obtain the approximate expression

$$\varphi(\eta) \approx \varphi(0) + \frac{\eta^2}{2} \quad (35)$$

corresponding to the parabolic SSS with the unknown $\varphi(0)$. However, this is only valid within a restricted range of η , where the exponentially growing factor in front of the integral in the LHS of Eq. (23a) is of no importance. As $\rho \exp(\eta^2/4)$ becomes of order unity, i.e., the value of $|\eta|$ approaches a critical value $\eta_0 \approx 2\sqrt{\ln(1/\rho)}$, the fast growing exponential factor starts overpowering the small parameter ρ , so that for sufficiently large $|\eta|$, the integral term in the LHS of Eq. (23a) becomes more important. The critical coordinates $|\eta| = \eta_0$

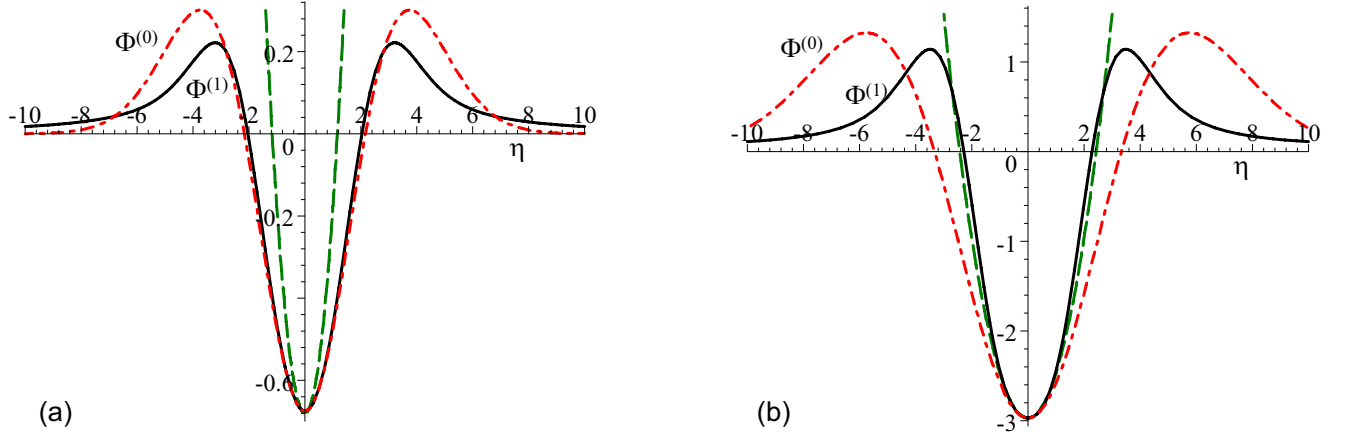


FIG. 9: Zero-order, $\varphi^{(0)}(\eta)$, and first-order, $\varphi^{(1)}(\eta)$, approximations: (a) $\rho = 1$ ($\lambda = 0.107$, $A = 0.675$); (b) $\rho = 0.1$ ($\lambda = 4.52 \times 10^{-2}$, $A = 2.97$). The dashed parabolic curves in the middle show the self-similar solution, $\varphi^{\text{ss}}(\eta) = \varphi(0) + \eta^2/2$.

are located slightly beyond the two maxima of the residual potential, where the parabolically growing potential of the major trail starts transforming to a decreasing potential beyond the trail.

The parameter η_0 is of major interest for us because it determines the rough boundary for the parabolic potential and hence for the maximum residual electric field responsible for the electron drift. Because the above heuristic estimate for η_0 was based on a simple order-of-magnitude comparison, we need a more accurate and consistent estimate. We will construct a piece-wise approximation for $\varphi(\eta)$, which would be close to the self-similar approximation given by Eq. (35) at $|\eta| \lesssim \eta_0$ and proportional to η^{-2} , Eq. (C21), at $|\eta| > \eta_0$. We will do this by iterations. As a zero-order approximation, $\varphi^{(0)}(\eta)$, we will set

$$\varphi^{(0)}(\eta) = \begin{cases} \varphi_0 + \frac{\eta^2}{2} & \text{if } |\eta| < \eta_0, \\ \left(\varphi_0 + \frac{\eta_0^2}{2}\right) \frac{\eta_0^2}{\eta^2} & \text{if } |\eta| > \eta_0, \end{cases} \quad (36)$$

with an unknown constant φ_0 . The function $\varphi^{(0)}(\eta)$ is a continuous function, while its derivative, $\partial_\eta \varphi^{(0)}(\eta)$, is discontinuous at $|\eta| = \eta_0$. As a next-order approximation, we will construct a smooth function $\varphi^{(1)}(\eta)$,

$$\varphi^{(1)}(\eta) = \begin{cases} \varphi_0 + \frac{\eta^2}{2} + \delta\varphi^{(1)}(\eta) & \text{if } |\eta| < \eta_0, \\ \left(\varphi_0 + \frac{\eta_0^2}{2} + \delta\varphi^{(1)}(\eta_0)\right) \frac{\eta_0^2}{\eta^2} & \text{if } |\eta| > \eta_0, \end{cases} \quad (37)$$

where the deviation from the self-similar solution, $\delta\varphi^{(1)}(\eta)$, can be found from Eq. (D6a) equivalent to Eq. (23a). Substituting $\varphi^{(0)}(\tau)$ for $\varphi(\tau)$ in the integral term, we obtain

$$\frac{d\delta\varphi^{(1)}}{d\eta} \approx -\frac{2\rho e^{\frac{\eta^2}{4}}}{\pi^{3/2}} \mathcal{P} \int_{-\infty}^{\infty} \frac{\varphi^{(0)}(\tau)}{\tau - \eta} d\tau = -\frac{\rho e^{\frac{\eta^2}{4}} I(\eta)}{\pi^{3/2}}, \quad (38)$$

where

$$I(\eta) = (\eta_0^2 - \eta^2) \frac{\eta_0^2 + 2\varphi_0 + \eta^2}{\eta^2} \ln \left| \frac{\eta_0 + \eta}{\eta_0 - \eta} \right| - \frac{2\eta_0 (\eta_0^2 - \eta^2 + 2\varphi_0)}{\eta}. \quad (39)$$

The function $\delta\varphi^{(1)}(\eta)$ is negative with the roughly exponentially growing absolute value. At $|\eta| = \eta_0$, we have

$$\left. \frac{d\delta\varphi^{(1)}}{d\eta} \right|_{\eta=\eta_0} = \frac{4\rho e^{\frac{\eta_0^2}{4}} \varphi_0}{\pi^{3/2}}, \quad (40)$$

which allows us to match the derivative of $\varphi^{(1)}$ at both sides of $|\eta| = \eta_0$,

$$\eta_0 + \frac{4\rho e^{\frac{\eta_0^2}{4}} \varphi_0}{\pi^{3/2}} = -\frac{2}{\eta_0} \left(\varphi_0 + \frac{\eta_0^2}{2} + \delta\varphi^{(1)}(\eta_0) \right). \quad (41)$$

Integrating Eq. (38), we obtain

$$\delta\varphi^{(1)}(\eta) = -\frac{\rho}{\pi^{3/2}} \int_0^\eta e^{\frac{\tau^2}{4}} I(\tau) d\tau, \quad (42)$$

where, notwithstanding the singular denominators in $I(\eta)$, the integrand at $\tau \rightarrow 0$ behaves regularly, $I(\tau) \propto \tau$. Assuming sufficiently large η_0^2 , to the first-order accuracy in the η_0^{-2} expansion, we obtain

$$\delta\varphi^{(1)}(\eta_0) \approx \frac{8\rho e^{\frac{\eta_0^2}{4}}}{\pi^{3/2} \eta_0} \left[\left(1 + \frac{6 - 2\tilde{\gamma} - 4 \ln \eta_0}{\eta_0^2} \right) \varphi_0 + 4 - 2\tilde{\gamma} - 4 \ln \eta_0 \right], \quad (43)$$

where $\tilde{\gamma} \approx 0.5772$ is the Euler constant. Substituting this to Eq. (41), we obtain the relation between ρ , η_0 , and φ_0 . To exclude the unknown constant φ_0 and determine ρ as a function of η_0 , we need one more equation. We will use the general relation $\int_0^\infty \varphi(\eta_0) d\eta = 0$, Eq. (D1), which is necessary for consistency of the Laplace equation in the far zone,

see Appendix B. Integrating the major parabolic part of the potential at $|\eta| < \eta_0$ in Eq. (37) is trivial, but integrating $\delta\varphi^{(1)}(\eta)$, Eq. (42), is complicated. Note, however, that integrating the major part gives rise to an additional large factor $\sim \eta_0$ and every next integration of $\delta\varphi^{(1)}(\eta)$ gives rise to an additional reduction factor $\sim \eta_0^{-2}$. While the derivative of $\delta\varphi^{(1)}$ at $|\eta| = \eta_0$, Eq. (38), is comparable to η_0 , the relative contributions of $\delta\varphi^{(1)}(\eta_0)$, and especially of its integral, are small compared to those from the major part. bearing this in mind, we obtain to the first-order accuracy with respect to η_0^{-2} ,

$$\rho \approx \frac{\pi^{3/2} e^{-\frac{\eta_0^2}{4}}}{\eta_0} \left(1 + \frac{2}{\eta_0^2}\right), \quad (44a)$$

$$\varphi_0 \approx -\frac{\eta_0^2}{3} + \frac{4}{3}, \quad (44b)$$

Application of other general relations, Eq. (D7), instead of Eq. (D1), yields somewhat different values of the first-order corrections. In Eq. (44a), we will disregard these corrections and obtain the solution of $\eta_0(\rho)$ in terms of the Lambert W-function, $W(x)$ [32]:

$$\eta_0 = \left[2W\left(\frac{\pi^3}{2\rho^2}\right)\right]^{1/2} \quad (45)$$

To logarithmic accuracy, we obtain

$$\eta_0 \simeq 2 \left\{ \ln \left[\frac{\pi^{3/2}}{2\rho\sqrt{\ln(\pi^{3/2}/\rho)}} \right] \right\}^{1/2} \simeq 2 \left(\ln \frac{1}{\rho} \right)^{1/2}, \quad (46)$$

in good agreement with the above heuristic estimate.

C. Trail diffusion

Given the approximate expressions for the residual potential, we will solve now the problem of trail diffusion described by Eqs. (10a) or (15a). While this treatment will require a number of approximations, the comparison with simulations described in Sect. VII shows that the analytical theory developed below is valid to a good accuracy.

For the strictly perpendicular case, $\theta = 90^\circ$, the self-similar solution (SSS) obtained in Appendix A is given by

$$n^{\text{SS}}(\xi, \zeta, t) \equiv \frac{N^{\text{SS}}}{N_0} \approx \frac{n_{\text{lin}}}{4\pi Dt} \left(\frac{1+\psi}{\psi} \right)^{1/2} \times \exp \left[-\frac{1}{4} \left(\frac{1+\psi}{\psi} \xi^2 + \zeta^2 \right) \right], \quad (47)$$

where $n_{\text{lin}} \equiv N_{\text{lin}}/N_0$ is the trail line density along the axis z normalized to the background plasma density. Under assumption that the initial maximum density is well above the background plasma density, $N_{\text{max}} \gg N_0$, the self-similar Gaussian profile can be used as a reasonable initial condition for

the density disturbance $\Delta n(t_0) = n(t_0) - 1$, as we did in our simulations,

$$\Delta n(t_0) \approx n^{\text{SS}}(t_0) = \Delta n_0 \exp \left[-\frac{1}{4} \left(\frac{1+\psi}{\psi} \xi^2 + \zeta^2 \right) \right],$$

$$\Delta n_0 = \frac{n_{\text{lin}}}{4\pi Dt_0} \left(\frac{1+\psi}{\psi} \right)^{1/2}. \quad (48)$$

Our numerical computations, starting from the initial condition $n_{\text{Trail}}(t_0) = n^{\text{SS}}(t_0)$ with $n_0 \gg 1$, show that, for some time, the trail density approximately follows the SSS. As the peak density decreases with increasing time, the solution starts to gradually deviate from the SSS. However, within the trail density peak, it keeps the nearly Gaussian form,

$$n_{\text{Trail}} = \frac{\Delta n_0 t_0}{t} \sqrt{\frac{q_0}{q(t)}} \exp \left[-\frac{1}{4} \left(\frac{\xi^2}{q(t)} + \zeta^2 \right) \right], \quad (49)$$

where the characteristic diffusion scale in the x direction ($\xi = x/\sqrt{Dt}$) is determined by a time-dependent coefficient $q(t)$ with the SSS initial condition,

$$q(t_0) = q_0 \equiv \frac{\psi}{1+\psi}. \quad (50)$$

In the original coordinates x and y , the nearly Gaussian peak can be expressed in terms of the x, y -dispersions, $\sigma_{x,y}$,

$$\sigma_x(t) = \langle x^2(t) \rangle \quad (51a)$$

$$\equiv \int_{-\infty}^{\infty} x^2 n_{\text{Trail}}(x, 0, t) dx / \int_{-\infty}^{\infty} n_{\text{Trail}}(x, 0, t) dx,$$

$$\sigma_y(t) = \langle y^2(t) \rangle \quad (51b)$$

$$\equiv \int_{-\infty}^{\infty} y^2 n_{\text{Trail}}(0, y, t) dy / \int_{-\infty}^{\infty} n_{\text{Trail}}(0, y, t) dy,$$

as

$$n_{\text{Trail}} = \frac{n_{\text{lin}}}{2\pi\sigma_x\sigma_y} \exp \left(-\frac{x^2}{2\sigma_x^2} - \frac{y^2}{2\sigma_y^2} \right). \quad (52)$$

The small residual electric field in the y direction (i.e., along \mathbf{B}_0) practically does not affect the SSS, $\sigma_y^2 = 2Dt$, because the parallel residual electric field is small, so that the diffusion along \mathbf{B}_0 is determined by the isotropic diffusion rate D , Eq. (11). At the same time, the strong residual electric field along x affects the diffusion in this direction, especially at altitudes above 93-97 ($\psi \lesssim 1$). The deviation of the characteristic trail size from that determined by isotropic diffusion is described in Eq. (49) by the coefficient

$$q(t) = \frac{\sigma_x^2(t)}{2Dt}. \quad (53)$$

The coefficient $q(t)$ slowly grows with time as the trail diffuses faster than it does in the SSS. As the electric field falls well below that predicted by the SSS (see Sec. VB), the diffusion becomes nearly isotropic, $q(t) \simeq 1$, determined in the two directions roughly by the same isotropic diffusion rate D .

The coefficient $q(t)$ is determined by the residual electric potential in the near zone. In the central part of the near zone, the potential along ξ , $\phi_{\text{res}}^0(\xi)$, always has a nearly parabolic behavior similar to the SSS, Eq. (A2),

$$\phi_{\text{res}}^0 - \phi_{\text{res}}^0(0) \approx \frac{B_{xx}\xi^2}{4}. \quad (54)$$

Unlike Eq. (A6), however, the coefficient B_{xx} in Eq. (54) is no longer a constant but changes with time. Our simulations show that the central region described by the nearly parabolic ξ -dependence is broad enough to include the entire trail peak. It is the parabolic behavior of the potential that imposes the Gaussian shape of the trail.

Substituting Eqs. (49) and (54) into the continuity equation (15a), we obtain a differential equation for $q(t)$,

$$t \frac{dq}{dt} = -(1 + B_{xx})q + 1, \quad (55)$$

which is not yet closed because the parabolic coefficient B_{xx} is itself an unknown function of $q(t)$. To determine it, we will use the solutions for the residual potential found in Sect. V B. These solutions are expressed in terms of renormalized variables φ and η defined by Eqs. (24). In these variables, the parabolic behavior of Eq. (54) is described by

$$\varphi(\eta) - \varphi(0) \approx \frac{F\eta^2}{2}. \quad (56)$$

Here the coefficient $F(\rho)$ is similar to B_{xx} . Unlike the latter, it depends upon one parameter ρ related to q by Eq. (25), $\rho(t) = \gamma q(t)t$. Comparing Eqs. (54) and (56) using (24) yields the relation $B_{xx}q = F(\rho)/(1 + \psi)$, which reduces Eq. (55) to a closed nonlinear differential equation for $\rho(t)$,

$$\frac{1}{\gamma} \frac{d\rho}{dt} = -\frac{F(\rho)}{1 + \psi} + 1. \quad (57)$$

Integrating Eq. (57) for $t(\rho)$ with the initial condition at $t = t_0$ given by $\rho(t_0) \approx \rho_0 \equiv \gamma q_0 t_0$,

$$\rho_0 = \frac{\gamma\psi t_0}{1 + \psi} = \frac{\sqrt{\psi}}{2(1 + \psi)\Theta_0 n_0} \ll 1, \quad (58)$$

Eq. (C14), we obtain for the general $F(\rho)$:

$$\gamma(t - t_0) = \int_{\rho_0}^{\rho} \frac{d\rho}{1 - F(\rho)/(1 + \psi)}. \quad (59)$$

During the initial time when $\rho(t) \ll 1$, both the trail density and the parabolic approximation of the potential follow the SSS, $B_{xx} \approx 1/\psi$, $q \approx q_0$, $F \approx 1$,

$$\rho(t) \approx \frac{\gamma\psi t}{1 + \psi}. \quad (60)$$

Using this, in Eq. (59) we can set $F = 1$ for $t \leq t_0$ and then replace t_0 and ρ_0 by zeroes. This corresponds to diffusion of the initially infinitely dense and thin (δ -function like) trail. The solution of $\rho(t)$ is determined by reversing Eq. (59). The

RHS of Eq. (59) is always positive, so that this reversal is unambiguous.

In the course of the trail diffusion, when the parameter ρ becomes of order unity and greater, the monotonically decreasing function $F(\rho)$ starts deviating from unity. To obtain the explicit expression for $F(\rho) = (1/\eta)(d\varphi/d\eta)$, we will use the solutions found in see Sect. V B. While we have no simple analytical expression for $F(\rho)$ for all ρ , we can approximate it by interpolating between $F \approx 1$ for $\rho \ll 1$, Eq. (35), and $F \approx 1/\rho$ at $\rho \gg 1$, Eq. (27). The simplest monotonic interpolation is

$$F(\rho) \approx \frac{1}{1 + \rho}. \quad (61)$$

Substituting this into Eq. (59) allows us to obtain the solution for $t(\rho)$:

$$\gamma t = \rho + \frac{1}{1 + \psi} \ln \left(1 + \frac{1 + \psi}{\psi} \rho \right). \quad (62)$$

Reversing this relation, we obtain an explicit expression for $\rho(t)$ in terms of the Lambert W -function,

$$\rho(t) = \frac{W(\psi e^{(1+\psi)\gamma t + \psi}) - \psi}{1 + \psi}. \quad (63)$$

This general expression describes the transition from the SSS for $\gamma t \ll 1$, Eq. (60), to

$$\rho(t) \approx \gamma t - \frac{1}{1 + \psi} \ln \left(\frac{1 + \psi}{\psi} \gamma t \right) \quad (64)$$

at large γt . According to Eqs. (25), (51b), and (53),

$$\sigma_x^2(t) = \frac{2D\rho(t)}{\gamma} = \frac{\sqrt{1 + \psi}\Theta_0 N_{\text{lin}}}{\pi N_0} \rho(t), \quad (65)$$

so that the first term on the RHSs of Eqs. (64) corresponds to diffusion over x with the isotropic rate D , while the second logarithmic term describes a small time delay. Since the trail diffusion along y has the same rate, $\sigma_y^2 \approx 2Dt$, the above expressions predict an evolution from anisotropic to isotropic diffusion.

The diffusion starts changing its character from the self-similar, sharply anisotropic diffusion to the nearly isotropic one roughly at a time $t = t_{\text{cr}}$ when $\rho(t_{\text{cr}}) = 1$. According to Eqs. (26) and (62), the corresponding critical time t_{cr} is given by

$$t_{\text{cr}} = \frac{N_{\text{lin}} e B_0 \mathcal{K}(\psi)}{2\pi (T_e + T_i) N_0} \approx 9.235 \times 10^{-2} \text{s} \left(\frac{B_0}{5 \times 10^4 \text{nT}} \right) \times \left(\frac{N_{\text{lin}}}{10^{14} \text{m}^{-1}} \right) \left(\frac{10^{11} \text{m}^{-3}}{N_0} \right) \left(\frac{1000 \text{K}}{T_e + T_i} \right) \mathcal{K}(\psi), \quad (66)$$

where

$$\mathcal{K}(\psi) = \sqrt{\frac{\psi}{1 + \psi}} \left[1 + \psi + \ln \left(\frac{1 + 2\psi}{\psi} \right) \right] \quad (67)$$

The critical transition time from anisotropic to isotropic diffusion is mostly relevant for high altitudes with $\psi \ll 1$, where the anisotropy of diffusion is clearly pronounced. In this case, the function $\mathcal{K}(\psi) \approx \sqrt{\psi}[1 + \ln(1/\psi)]$. According to Eq. (2), $\sqrt{\psi} \propto N_n B_0^{-1}$. From Eq. (66) we see that t_{cr} is practically independent of the magnetic field, making the high and low latitude diffusion evolve similarly. The altitudinal dependence of t_{cr} , however, depends strongly on the background plasma density N_0 and even more so on the neutral density N_n .

D. Density disturbances beyond the trail

The residual electric potential originated within the trail and extended along the magnetic density creates disturbances in the background plasma, as we observed in our numerical calculations, see Sect. IV, Feature 3. These density disturbances occur due to the fact that the extended residual potential attracts ions from the surrounding ionosphere into the central part with the deep potential minimum around $x = 0$. This results in plasma compression in the central potential minimum and depletion in the adjacent regions where the residual potential has two symmetric maxima.

In this section, we will estimate density disturbances in the background plasma beyond the trail. One motivation for this is that when obtaining the equation for the residual potential in the near zone, Eq. (23), we have completely neglected these disturbances. This has allowed us to reduce the equation for the residual potential in the far region to the Laplace equation in renormalized coordinates, see Eq. (B1) in Appendix B. To estimate the effect of density disturbances, we will consider the strongest case of dense trail described in Sect. VB 3. Another motivation is to find a proper adjustment for the parameter ρ , which is needed for the residual potential at sufficiently large state of trail diffusion.

1. Strongest case, $\rho \ll 1$: justification of analytical approach

To justify the neglect of density disturbances beyond the trail, see Appendix B, we will make a simple analytical estimate of density disturbances beyond the trail. The largest disturbances beyond the trail occur in the near zone in the early stage of dense-trail diffusion, $\rho \ll 1$.

Given the spatial distribution of the residual potential ϕ_{res} , the dynamics of density perturbations is described by Eq. (10a). If we assumed a stationary regime, $\partial_t n = 0$, then imposing boundary conditions at infinity where $n \rightarrow 1$ and $\phi_{\text{res}}^0 \rightarrow 0$ we would obtain the local Boltzmann distribution of plasma density, $n = \exp(-\phi_{\text{res}}^0)$. In the strongest case of $\rho \ll 1$, according to Eq. (44b), the potential minimum is $\varphi_0 \simeq -\eta_0^2/3$, so that according to Eq. (24a) the corresponding potential $\phi_{\text{res}} \approx \phi_{\text{res}}^0 = \varphi_0/2(1 + \psi) \simeq -\eta_0^2/[6(1 + \psi)]$. For sufficiently small ρ , the parameter η_0 depends logarithmically on ρ and may reach several units, Eq. (46). In this case, the local Boltzmann distribution would yield disturbances of the background plasma near the trail much greater than the

background density itself, $n \sim 1/\rho \gg 1$, making the assumption underlying our theoretical approach to be invalid. Fortunately, our numerical simulations, even in the cases as strong as $n_{\text{max}} = 10^4$, have shown that the background density disturbances are at worst of order unity in the central near zone and are much less beyond it, as described in Sect. IV. The physical reason for this is that the trail diffusion is a non-stationary process with a diffusion prehistory. Plasma density disturbances caused by the potential expanding with time prove to be noticeably smaller than those caused by the stationary potential.

For a simple estimate of plasma density disturbances outside the trail in the non-stationary process, we linearize Eq. (10a) for relatively small density disturbances, $\delta n = \delta N/N_0 \equiv n - 1$. In accord with our theory and simulations, we also assume that the major gradients beyond the trail are perpendicular to the magnetic field, i.e., are directed mainly along the x coordinate. As a result, we obtain from Eq. (10a) a simpler equation,

$$\partial_t \delta n - D \partial_{xx}^2 \delta n = D \partial_{xx}^2 \phi_{\text{res}}(x, t). \quad (68)$$

Solving this linear equation via the proper Green function and performing integration by parts, we obtain

$$\begin{aligned} \delta n(x, t) = & \sqrt{\frac{1}{16\pi D}} \int_{t_0}^t \frac{d\tilde{t}}{(t - \tilde{t})^{3/2}} \\ & \times \int_{-\infty}^{\infty} (\tilde{x} - x) \exp\left[-\frac{(\tilde{x} - x)^2}{4D(t - \tilde{t})}\right] \partial_{\tilde{x}} \phi_{\text{res}}(\tilde{x}, \tilde{t}) d\tilde{x}. \end{aligned} \quad (69)$$

This expression shows that general density disturbances are determined by the entire distribution of the residual electric field over \tilde{x} from all previous times \tilde{t} . It is straightforward to check that for stationary ϕ_{res} and $t \gg t_0$, Eq. (69) reduces to dependence $\delta n(x, t) = -\phi_{\text{res}}(x, t)$ corresponding to the local Boltzmann distribution for $\phi_{\text{res}} \ll 1$.

Before applying a specific model for $\partial_{\tilde{x}} \phi_{\text{res}}(\tilde{x}, \tilde{t})$ we note the following. When the local coordinate \tilde{x} varies from 0 to ∞ , the residual electric field $-\partial_{\tilde{x}} \phi_{\text{res}}(\tilde{x}, \tilde{t})$ changes its sign. In the central region it draws plasma to the center, while outside the central region it repels it. At any previous time $\tilde{t} < t$, the local density disturbances are determined by integral contributions from the two competing regions that generally do not balance each other. In the absence of the exponential factor in the RHS of Eq. (69), according to Eq. (D2), the two contributions would exactly compensate each other. The exponential factor, however, breaks the balance. For example, in the center, $x = 0$, the attraction always dominates, so that the total density disturbance there is positive (plasma compression). In the adjacent regions, the situation is opposite, so that the repulsion dominates there, resulting in plasma depletion.

The strongest density disturbances are within the near zone, where the potential reaches its absolute minimum. For simple estimate of the potential φ in the early stage of trail diffusion, $\rho \ll 1$, we choose its zero-order approximation, $\varphi^{(0)}$, Eq. (36), so that $\phi_{\text{res}} \approx \phi_{\text{res}}^0 \approx \varphi^{(0)}/2(1 + \psi)$. Recalling the definition of the renormalized coordinate η , Eq. (24b), and

renormalizing the local time variable \tilde{t} , we obtain

$$\partial_{\tilde{x}}\phi_{\text{res}}(\tilde{x}, \tilde{t}) = \frac{1}{2\psi} \times \begin{cases} \frac{\omega}{\sqrt{\tau}} & \text{if } \left| \frac{\omega}{\sqrt{\tau}} \right| < \eta_1 \\ -\frac{\eta_1^4}{3} \left(\frac{\sqrt{\tau}}{\omega} \right)^3 & \text{if } \left| \frac{\omega}{\sqrt{\tau}} \right| > \eta_1 \end{cases}, \quad (70)$$

where

$$\tau \equiv \frac{\tilde{t}}{t}, \quad \eta_1 \equiv \sqrt{\frac{\psi}{1+\psi}} \eta_0. \quad (71)$$

We restrict our analytic estimate to the center, $x = 0$, where we expect the largest positive density disturbances, and assume $t \gg t_0$. As a result, performing the integration over space, we obtain from Eqs. (69) and (70)

$$\delta n(0, t) \approx \frac{1}{8\psi\sqrt{\pi}} \int_0^1 (I_1 - I_2) d\tau, \quad (72)$$

where

$$I_1 = \frac{2\sqrt{\pi}}{\tau} \operatorname{erf}\left(\frac{\eta_1\sqrt{\tau}}{2\sqrt{1-\tau}}\right) - \frac{2\eta_1}{\sqrt{\tau(1-\tau)}} \exp\left(-\frac{\eta_1^2\tau}{4(1-\tau)}\right), \quad (73a)$$

$$I_2 = \frac{\eta_1^4\tau\sqrt{\pi}}{6(1-\tau)^2} \left[\operatorname{erf}\left(\frac{\eta_1\sqrt{\tau}}{2\sqrt{1-\tau}}\right) - 1 \right] + \frac{\eta_1^3\tau^{1/2}}{3(1-\tau)^{3/2}} \exp\left(-\frac{\eta_1^2\tau}{4(1-\tau)}\right) \quad (73b)$$

are positive functions of τ and $I_2(\tau) < I_1(\tau)$.

For small η_1 , which for $\eta_0 \sim 3-5$ is possible only at sufficiently high altitudes where $\psi \ll \eta_0^{-2}$, the two functions are mainly localized near $\tau = 1$ ($\tilde{t} \simeq t$). As a result, we obtain $\int_0^1 I_1 d\tau \approx \eta_1^2\sqrt{\pi}/2$ and $\int_0^1 I_2 d\tau \approx \eta_1^2\sqrt{\pi}/3$, so that in this case $\delta n(0, t) \simeq \eta_0^2/50$. Under real physical conditions, the value of η_0 can reach several units, so that the maximum density disturbance of the background plasma in the near zone is of order unity. The largest value of density disturbances observed in our simulations was $\delta n(0, t) \simeq 2$, which is larger than those following from the linearized Eq. (68) but is of the same order of magnitude.

At lower altitudes, $\psi \gtrsim 1$, according to Eq. (71), the value of η_1 is not small but is always less than η_0 . As the value of $\eta_1 > 1$ grows, the maxima of $I_{1,2}$ shift to smaller values of τ . This means that the density disturbances at a given time t become more affected by electric fields at past time, $\tilde{t} < t$. In addition, the ratio I_2/I_1 becomes smaller, which means that the effect of the oppositely directed electric field beyond the major region of the potential distribution, $\omega/\sqrt{\tau} > \eta_1$, Eq. (70), becomes less important. For $\eta_1 \gg 1$, $\int_0^1 I_1 d\tau \simeq 4\sqrt{\pi} \ln \eta_1$. The value of $\eta_1 < \eta_0$, however, can reach 3-4 as a maximum (at sufficiently large ψ corresponding to lower altitudes). In this case, the integral $\int_0^1 (I_1 - I_2) d\tau \lesssim \int_0^1 I_1 d\tau$ can reach several units at most, so that $\delta n(0, t)$ should remain small.

These simple estimates confirm our numerical observations that even in the strongest cases the relative plasma density

disturbances in the near zone are of order unity at worst, see Fig. 6. In all other situations or locations, such as for $\rho \gtrsim 1$, $t \sim t_0$, etc., and especially in the far zone where the major current closure takes place, the density disturbances are much smaller. This shows that our basic theoretical scheme which relies on the Laplace equation for the electric potential in the far zone and neglects density disturbances is a reasonable approximation.

2. Weakest case, $\rho \gg 1$: adjustment of ρ for residual potential

The simulations show that Eq. (63) describes well the evolution of the simulated trail density for all parameters ρ , while the residual potential solution described in Sect. V B shows a discrepancy for the late diffusion stage when ρ is large. To fit the evolution of the simulated potential, the expression for the master parameter ρ given by Eq. (63) needs an adjustment $\rho(t) \rightarrow \tilde{\rho}(t)$ corresponding to an effective time lag. We argue that small background density disturbances beyond the trail are responsible for this discrepancy.

To estimate background plasma density disturbances in the later stage of trail diffusion, we will use the zeroth-order approximation for the residual potential given by Eq. (30). In the limit of $\rho \gg 1$, when $\rho(t) \simeq \gamma t$, we have in the near zone

$$\phi_{\text{res}}^0(x, t) \simeq \frac{I(x/\sqrt{Dt})}{2(1+\psi)\rho(t)}, \quad (74)$$

where

$$I(z) = -e^{-\frac{z^2}{6}} \left(1 - \frac{z^2}{3}\right).$$

Substituting Eq. (74) for $x = 0$ into Eq. (69), we obtain

$$\delta n(x, t) \simeq \frac{1}{2(1+\psi)\rho(t)}. \quad (75)$$

Thus for $\rho \gg 1$ the background density disturbances are small, justifying the use of Eqs. (68) and (69).

We will use Eq. (75) to reconcile the discrepancy described above. One of the key factors in the derivation of the governing equation for the near-zone potential, Eq. (23), has been the calculation of the density disturbance integral over the effective ζ -region in the near zone, ΔN_{ζ_1} , as described in Appendix C. This effective region includes the trail with a nearly constant φ_{res} and an adjacent region where a noticeable ζ -derivative of φ_{res} builds up, as seen in Fig. 5 at $y \simeq -10$. This derivative defines the fields and current closure structure in the far zone. The effective integral ΔN_{ζ_1} should include both the trail density and the disturbances of the background plasma. The calculation of Appendix C took into account only the former and completely neglected the latter. For a dense trail with $\rho \ll 1$, this proves to be justified because the relative contribution of the background plasma disturbances to the integral proves to be small compared to the contribution of the trail density. On the contrary, for a much less dense trail with $\rho \gg 1$, the contribution of background density disturbances becomes comparable to that from the trail density.

In Appendix F, we have obtained the effective integral $\Delta N_{\zeta_1}(\xi)$ and the relation between $\tilde{\rho}$ and ρ in terms of two coupled parameters of order unity, $\beta(\rho)$ and $\tilde{\beta}(\rho)$, Eqs. (F5) and (F6). Being unable to obtain these parameters analytically, we have used our simulations for $\psi \geq 0.05$ to obtain approximate Eq. (F8). For smaller ψ , we proposed Eq. (F9), which represents a conjecture and needs a special study.

VI. SUMMARY OF ANALYTICAL RESULTS

In this Section, we summarize our major analytical results which can be directly applied in comparisons with observations. To use the theoretical results for practical applications, we need to pass from the renormalized variables of Sect. V to the original ones. Where appropriate, we will use simplified versions of analytic expressions.

The original residual potential $\phi_{\text{res}}(x, y, t)$ is defined in Eq. (4). According to Eq. (24), the original residual potential in the near zone, $\phi_{\text{res}}^0(x, t) \equiv \phi_{\text{res}}(x, 0, t)$, in terms of the actual coordinate x and time t , is given by

$$\phi_{\text{res}}^0(x, t) = \frac{1}{2(1+\psi)} \varphi \left(\sqrt{\frac{\gamma}{D\rho(t)}} x, \rho(t) \right), \quad (76)$$

where γ is defined by Eq. (26). Assuming the E-region conditions, $\nu_{en} \simeq 10\nu_{in}$ and $m_i \simeq 30m_p$, we write γ in a form convenient for comparison with our FlexPDE simulations, Sect. IV where $n_0 = N_{\text{Trail}}(t_0)/N_0$ and $D = 1$,

$$\gamma = \frac{1}{2\Theta_0 \Delta n_0 t_0 \sqrt{\psi}} \simeq \frac{37.1}{\Delta n_0 t_0 \sqrt{\psi}}. \quad (77a)$$

In terms of the trail line density N_{lin} , background plasma density N_0 , temperatures $T_{e,i}$, and geomagnetic field B_0 , we express γ and the diffusion coefficient D as

$$\begin{aligned} \gamma &= \frac{2\pi N_0 (T_e + T_i)}{\sqrt{\psi(1+\psi)} N_{\text{lin}} e B} \\ &\simeq \frac{1.08 \times 10^{-2}}{\sqrt{\psi(1+\psi)}} \left(\frac{T_e + T_i}{1000\text{K}} \right) \left(\frac{0.5 \times 10^{-4}\text{T}}{B_0} \right) \\ &\times \left(\frac{N_0}{10^{10}\text{m}^{-3}} \right) \left(\frac{10^{14}\text{m}^{-1}}{N_{\text{lin}}} \right) \text{s}^{-1}, \end{aligned} \quad (77b)$$

$$D = \frac{T_e + T_i}{m_i \nu_{in}} \simeq \frac{23.2}{\sqrt{\psi}} \left(\frac{T_e + T_i}{1000\text{K}} \right) \left(\frac{0.5 \times 10^{-4}\text{T}}{B_0} \right) \text{m}^2 \text{s}^{-1}. \quad (77c)$$

The only time dependence in ϕ_{res}^0 is associated with the dimensionless parameter $\rho(t)$. The function $\varphi(\eta, \rho)$ has different approximate expressions depending upon the range of ρ , as described in Sect. VB. This parameter monotonically varies from small values in the early diffusion stage to large ones in the later diffusion stage. According to Eqs. (62) and (63), the time dependence of ρ can be approximately determined by

$$\gamma t = \rho + \frac{1}{1+\psi} \ln \left(1 + \frac{1+\psi}{\psi} \rho \right), \quad (78)$$

or, in the explicit form,

$$\rho(t) = \frac{W(\psi e^{(1+\psi)\gamma t + \psi}) - \psi}{1+\psi}, \quad (79)$$

where $W(x)$ is the Lambert W-function.

To calculate the residual potential for sufficiently large ρ , the parameter ρ needs an adjustment, $\rho \rightarrow \tilde{\rho} < \rho$,

$$\tilde{\rho}(\rho) = \frac{\rho}{2} \left(1 - \tilde{\beta}(\rho) + \sqrt{1 - 2\tilde{\beta}(\rho)} \right), \quad (80)$$

where

$$\tilde{\beta}(\rho) \approx \frac{0.92\rho}{(1+\psi)(2.2+\rho)} \sqrt{\frac{\gamma t}{\pi\rho}}, \quad \text{for } \psi \geq 0.05, \quad (81a)$$

$$\tilde{\beta}(\rho) \approx \frac{\rho}{2(2.2+\rho)} \sqrt{\frac{\gamma t}{\rho}}, \quad \text{for } \psi < 0.05, \quad (81b)$$

and the relationship between γt and ρ is given by Eq. (78). Equation (81a) includes the approximation for $\tilde{\beta}(\rho)$, Eq. (F8), obtained by fitting FlexPDE runs for $\psi \geq 0.05$, while Eq. (81b) is an extrapolation to smaller ψ .

In the earlier stage of dense-trail diffusion when $\rho(t) \approx \psi\gamma t/(1+\psi) \ll 1$, a simple approximation for the near-zone potential is given by the piece-wise function, Eq. (36),

$$\phi_{\text{res}}^0(x, t) \simeq \frac{1}{2(1+\psi)} \times \begin{cases} -\frac{\eta_0^2}{3} + \frac{\eta^2}{2} & \text{if } |\eta(x, t)| < \eta_0, \\ \frac{\eta_0^4}{6\eta^2} & \text{if } |\eta(x, t)| > \eta_0, \end{cases} \quad (82)$$

where $\eta(x, t) = x[\gamma/D\rho(t)]^{1/2}$ and $\eta_0 \simeq 2[\ln(1/\rho(t))]^{1/2}$.

For simple estimates of the residual potential near the trail at a later stage, $\rho(t) \sim \gamma t \gtrsim 1$, one can use the zero-order Eq. (30). To compare with simulations, however, we should use the more complicated, but more accurate, first-order Eq. (31), and replace ρ by $\tilde{\rho}$, Eq. (80), and η by $\tilde{\eta}(x, t) = x[\gamma/D\tilde{\rho}(t)]^{1/2}$,

$$\begin{aligned} \phi_{\text{res}}^0(x, t) &= \frac{1}{2(1+\psi)\tilde{\rho}(t)} \\ &\times \left\{ S(\tilde{\eta}) - \frac{2\lambda(\tilde{\rho})A(\tilde{\rho})}{\sqrt{1+4\lambda(\tilde{\rho})}} \left[\frac{4\lambda(\tilde{\rho})}{1+4\lambda(\tilde{\rho})} \right. \right. \\ &\left. \left. + (3-2\lambda(\tilde{\rho})\tilde{\eta}^2) S(\tilde{\eta}\sqrt{1+4\lambda(\tilde{\rho})}) \right] \right\}, \end{aligned} \quad (83)$$

where the functions S , λ , and A are defined by Eqs. (C17) and (34). Given $\phi_{\text{res}}^0(x, t)$, the residual potential in all locations is given by Eq. (B4). At large distances from the trail, $x^2 + \alpha^2 y^2 \gg Dt$, according to Eqs. (B5) and (25), the residual potential has a 2D quadrupole structure,

$$\phi_{\text{res}}(x, y, t) \approx \frac{C_1(\rho) \rho D (x^2 - \alpha^2 y^2)}{2(1+\psi)\gamma(x^2 + \alpha^2 y^2)^2}, \quad (84)$$

where $C_1(\rho) = \lim_{|\eta| \rightarrow \infty} [\eta^2 \varphi(\eta, \rho)]$, Eq. (D3).

The expression for the trail density is much simpler than those for the potential. According to Eq. (49) with $q = \rho/\gamma t$, Eq. (25), for all values of ρ it has a nearly Gaussian form,

$$\Delta n_{\text{Trail}}(x, y, t) \approx \Delta n_0 \sqrt{\frac{t_0 \rho_0}{t \rho(t)}} \exp \left[-\frac{1}{4D} \left(\frac{\gamma x^2}{\rho(t)} + \frac{y^2}{t} \right) \right], \quad (85)$$

where $\rho_0 \equiv \rho(t_0) \approx \gamma \psi t_0 / (1 + \psi)$, Eq. (58), and no adjustment for all ρ .

Eliminating t from Eqs. (78) and (85), we express the peak Gaussian density, $\Delta n_{\text{Peak}} \equiv \Delta n_{\text{Trail}}(0, 0, t)$, in terms of $\rho(t)$,

$$\Delta n_{\text{Peak}} = \left\{ 2\Theta_0 \sqrt{\rho \left[(1 + \psi) \rho + \ln \left(1 + \frac{1 + \psi}{\psi} \rho \right) \right]} \right\}^{-1}, \quad (86)$$

while the same quantity in the self-similar solution is given by

$$\Delta n_{\text{Peak}}^{\text{SS}} = \left\{ 2\Theta_0 \sqrt{\psi} \left[\rho + \frac{1}{1 + \psi} \ln \left(1 + \frac{1 + \psi}{\psi} \rho \right) \right] \right\}^{-1}. \quad (87)$$

These expressions have a universal form independent of the initial conditions, provided $t > 2t_0$ and $\Delta n(t_0) \gg 1$.

VII. COMPARISON OF THEORY AND SIMULATIONS

In this Section, we compare our analytical theory with simulations outlined in Sect. IV. We start with comparison of our simulations with the theoretical expression for the trail density, Eq. (85). In the early stage of dense-trail diffusion, $\rho \ll 1$, the nearly Gaussian peak in simulations closely follows the self-similar solution (SSS), Eq. (47), though it shows a slightly faster diffusion, as seen in Fig. 10(a). The density predicted by Eq. (85) is closer to the SSS curve than to the numerical one because the interpolation expression for $\rho(t)$ given by Eq. (63) is less accurate for $\rho \ll 1$ than it is for $\rho \gtrsim 1$.

When $\rho \sim 1$, the analytic solution for the density peak given by Eq. (85) starts deviating from the SSS and becomes closer to the numerical solution, as illustrated in Fig. 10(b). When ρ becomes larger, $\rho \gg 1$, the analytical theory shows an excellent agreement with simulations, while the SSS predicts a noticeably slower diffusion, as shown in Figs. 10(c) and (d).

Figure 11 shows the peak trail densities vs. ρ taken from the simulations, analytical theory, and self-similar solution. The numerical solution is shown by separate groups of points taken from several different runs (each group has its own point shape). Each run started at $t_0 = 1$ with different values of the initial peak trail density. In each group, consecutive points correspond to equidistant moments of time: $t = 1, 2, 3, \dots$. The first point of the group always lies on the dashed curve corresponding to Eq. (87) because the SSS was the initial condition for each run. However, starting from $t = 2$, the numerical points closely approach the theoretical curve given

by Eq. (86), while the SSS solution given by Eq. (87) remains noticeably offset. The theoretical curve overlays the numerical points for $\rho \gtrsim 1$, while for $\rho \ll 1$ it shows a slight deviation from the numerical points (see the beginning of this Section). The transition from an anisotropic diffusion to a more isotropic one occurs near the inflection point about $\rho = 1$. Notice that this takes place when the trail peak density remains well above the background plasma density, $\Delta n_{\text{max}} \sim (\Theta_0 \sqrt{\psi})^{-1} \simeq 80$ for $\psi = 0.05$.

Now we compare with simulations the theoretical expressions for the residual potential in the near zone. Figure 12 shows the residual potential along x for the same conditions as in Fig. 10. Because the parameter ρ spans a broad range of values from small to large ones we will apply either Eq. (82) or Eq. (83). Figure 12(a) shows that for $\rho \ll 1$ the simple piece-wise approximation agrees reasonably with simulations in all areas not too close to the two positive bumps of the potential. Indeed, while there is a significant difference between the values of the potential minimum at $x = 0$, the potential derivative (the residual electric field) is the same in the inner region characterized by the parabolic dependence and occupied by the trail, see Fig. 10(a). On the other hand, a good agreement also exists well beyond the trail, where the residual potential decreases with increasing $|x|$ and the corresponding electric field changes its sign. The zero-order piece-wise approximation is rough in the transitional zone near the two potential maxima, where it has a discontinuity in the electric field. The maximum electric fields in the piece-wise formula are reached near the discontinuity points, approaching them from inside. The maximum electric fields in simulations are reached at some locations in the inner region closer to the center and hence have smaller values. Thus the simple analytical formula yields nearly correct electric fields everywhere except the transitional zones between the inner and outer regions, where it overestimates the electric field magnitude. We have attempted modeling the transitional electric field with higher-order interpolations to provide a smooth transition, but this underestimated the field. The error for the maximum electric field, however, remains within the range of tens percent for all our simulations.

For $\rho \sim 1$, the theoretical expression given by Eq. (83) with unadjusted ρ ($\tilde{\rho} \rightarrow \rho$), agrees well with simulations practically in all locations, as seen in Fig. 12(b). As ρ becomes large, Eq. (83) with unadjusted ρ shows a significant discrepancy, as seen in Fig. 12(c) and (d). However, if we adjust the parameter ρ , $\rho \rightarrow \tilde{\rho}$ based on matching of the potential minima for the two solutions and apply Eq. (83) then the discrepancy practically disappears. It is important that the analytical solution with only one adjusted parameter $\rho \rightarrow \tilde{\rho}$ causes the theoretical ϕ_{res}^0 to match the numerical solution well not only near the potential minimum but everywhere. The relation between ρ and $\tilde{\rho}$ based on our simulations results in the empirical ρ -dependent adjustment coefficient β , Eqs. (80) and (81). We emphasize that the adjusted parameter $\tilde{\rho}$ is only needed for the residual potential and not for the trail density, as described in Sect. VD.

In this Section, we showed the comparison of theory and simulations mainly for small ψ . For large values of ψ , the trail

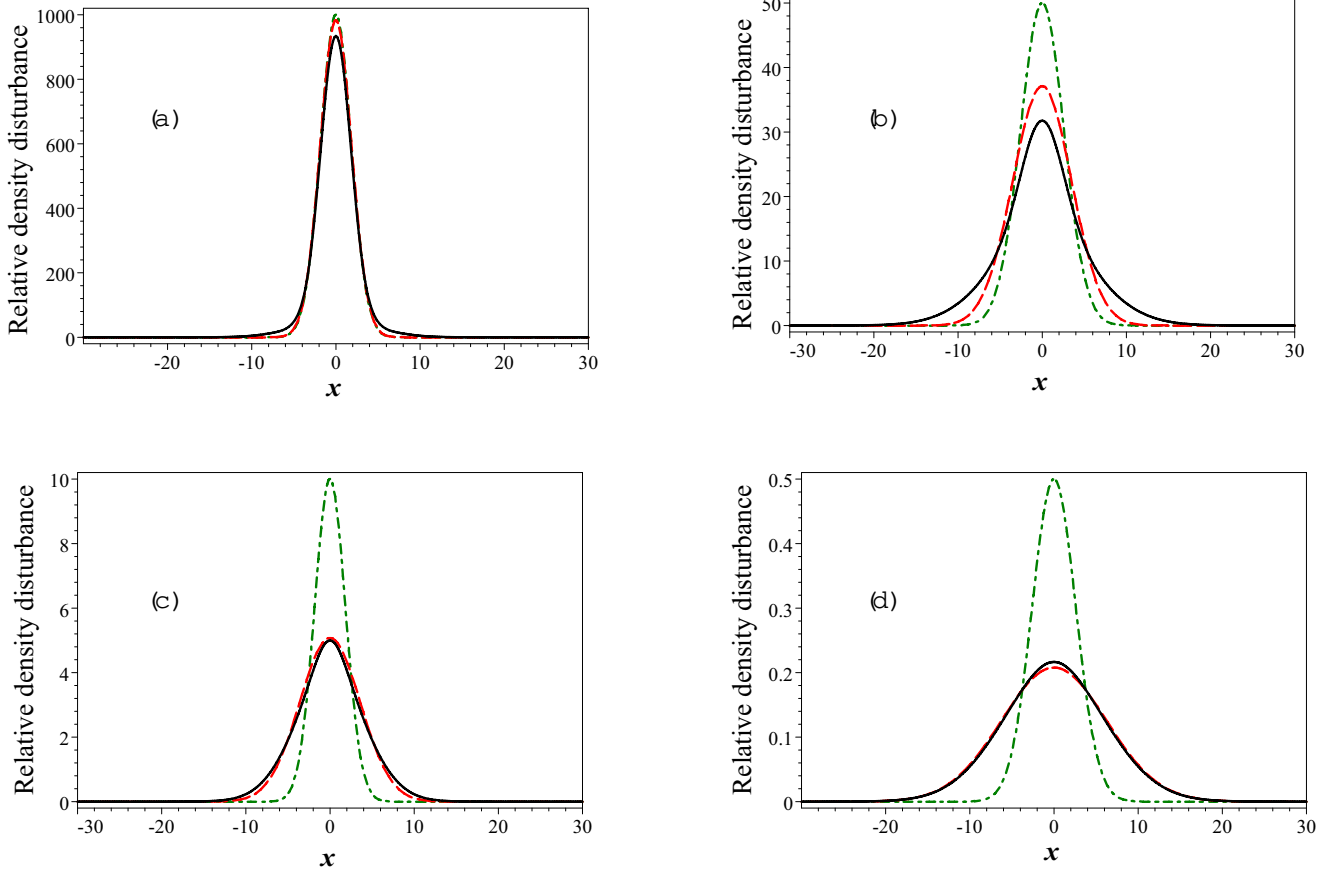


FIG. 10: Trail density distribution along x for $\psi = 0.2$. (a): $\Delta n_0 = 10^4$, $t = 10$, $\rho \approx 1.4 \times 10^{-3}$. (b): $\Delta n_0 = 1000$, $t = 20$, $\rho \approx 0.5$. (c): $\Delta n_0 = 100$, $t = 10$, $\rho \approx 5.37$. (d): $\Delta n_0 = 10$, $t = 20$, $\rho \approx 160$. Solid curves: the numerical solution; dot-dashed curves: the self-similar solution, Eq. (47); dashed curves: the analytical solution, Eq. (85).

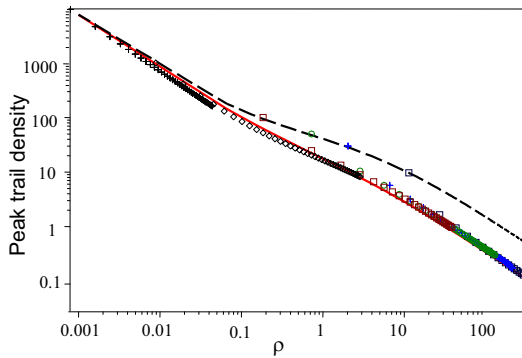


FIG. 11: Peak trail density vs. parameter ρ for $\psi = 0.05$. Points shown as alternating crosses, diamonds, boxes, and circles represent the numerical solution from several runs: $\Delta n_0 = 10^4, 10^3, 100, 50, 30, 10$. For each run, the consecutive points (from left to right) correspond to $t/t_0 = 1, 2, 3, \dots$. Solid curve shows the analytical solution given by Eq. (86). Dashed curve shows the self-similar solution given by Eq. (87).

diffusion in all stages of trail diffusion was nearly isotropic with small values of the residual electric field, in full accord with the analytical theory.

VIII. DISCUSSION

In this section, we will start by discussing some caveats, then we will estimate the induction electric field in the plasma trail, and finally we will dwell on plasma instabilities.

A. Caveats

In our theory, we have made a number of assumptions which are not perfectly valid. Among those were assumptions about constant electron and ion temperatures and about one sort of ions. However, the initially hot temperatures of the newly produced meteor trail plasma need some time for cooling. Also, this plasma includes material different from the ambient atmosphere, so that there may be at least two kinds of ions with different masses. We will include these factors in future work.

We also note that our full analytical theory has been developed only for the particular case of a mutually orthogonal

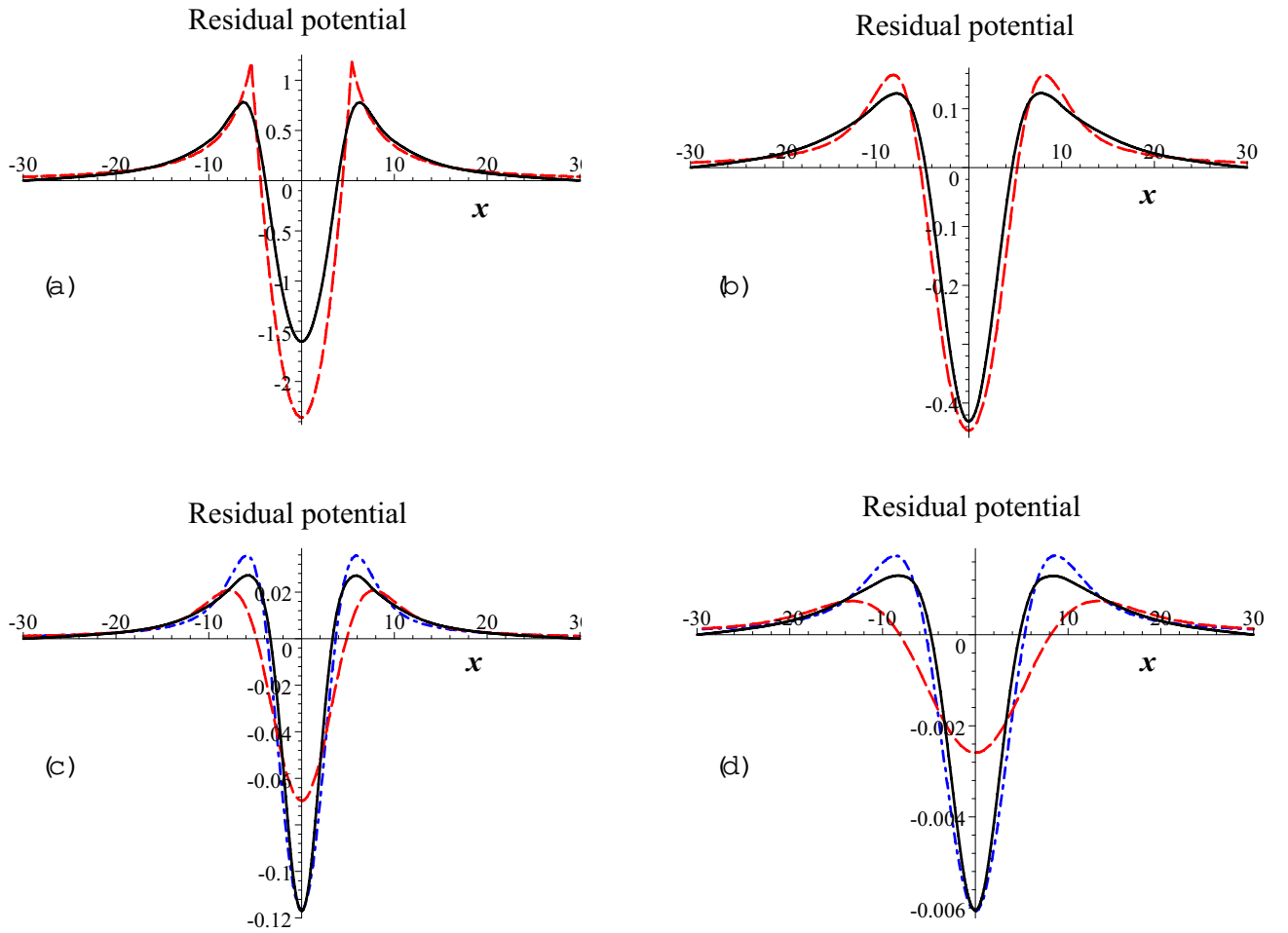


FIG. 12: Residual potentials at $y = 0$, $\phi_{\text{res}}^0(x, t)$, corresponding to density distributions in Fig. 10. Solid curves show the numerical solutions, while dashed and dot-dashed curves show the analytical solutions according to different equations. (a): $\Delta n_0 = 10^4$, $t = 10$, $\rho \approx 1.4 \times 10^{-3}$, dashed curve corresponds to Eq. (82). (b): $\Delta n_0 = 1000$, $t = 20$, $\rho \approx 0.5$, dashed curve corresponds to Eq. (83) with $\tilde{\rho} \rightarrow \rho$. (c): $\Delta n_0 = 100$, $t = 10$, $\rho \approx 5.37$, dashed curve corresponds to Eq. (83) with $\tilde{\rho} \rightarrow \rho$, dot-dashed curve corresponds to Eq. (83) with $\tilde{\rho} \approx 3$. (d): $\Delta n_0 = 10$, $t = 20$, $\rho \approx 160$, dashed curve corresponds to Eq. (83) with $\tilde{\rho} \rightarrow \rho$, dot-dashed curve corresponds to Eq. (83) with $\tilde{\rho} \approx 68$.

meteor trail axis and magnetic field, $\theta = 90^\circ$. A more general situation occurs when the angles between the trail axis and \mathbf{B}_0 , θ , are arbitrary but satisfy restrictions given by Eq. (7). It is only discussed for the self-similar solution described in Appendix A. If we ignore the effect of electron Hall currents into the process of the meteor trail diffusion then we can apply all our results where according to Eq. (12) the quantity α^{-1} , Eq. (B2), and the numerator of ρ , Eq. (25), acquire an additional factor $\sin \theta$. Our preliminary numerical computations show that the electron Hall current at $\theta \neq 90^\circ$ affects the meteor trail diffusion in such a way that the trail density contours become more isotropic and rotated at a small angle in the x, y plane, as the SSS does (see Appendix A).

B. Induction electric field

Now we estimate the induction electric field associated with the meteor plasma trail currents and show that, except for extraordinarily high-density meteors, this field is negligible. This is of importance for the electrostatic field approximation employed in our approach. The induction electric field may only occur due to disturbances of the magnetic field, $\delta \mathbf{B}$,

which in turn are due to the electric current, \mathbf{j} , caused by the plasma trail diffusion. Note that the magnetic field disturbances, even in spite of their extreme weakness, can be observable using a sophisticated measurement technique for diagnostics purposes. Furthermore, the initial formation of the trail current may have caused ELF/VLF signals observed on the ground and correlated with the meteor showers [24, 25].

According to the Maxwell equations, we have

$$\nabla \times \mathbf{E} = -\partial_t \delta \mathbf{B}, \quad (88a)$$

$$\nabla \times \delta \mathbf{B} = \mu_0 \mathbf{j}, \quad (88b)$$

where μ_0 is the permeability of free space and we neglected the displacement current (all characteristic speeds in the trail diffusion are much less than the speed of light, etc.). The net electric current is due to the fact that electrons and ions have different responses to the external force. Being proportional to the plasma density, the net electric current is mainly concentrated within the trail. It is predominantly formed by the unbalanced $\mathbf{E} \times \mathbf{B}$ drift of electrons. In the strongest case, the trail density behaves roughly in accord with the self-similar solution, so that for a simple estimate we can use the corresponding expressions for the current given by Eq. (A10). This

current with the density $j_z = (e\Omega_e x \sin \theta / 2\nu_{en} t) N^{\text{ss}}$, $N^{\text{ss}} = (C/t) \exp\{-[(1+\psi)x^2/\psi + y^2]/4Dt\}$, Eqs. (A1) and (A6), is directed along the trail axis and flows in opposite directions in the two halves of the trail, $x > 0$ and $x < 0$ (in the actual 3D, spatially inhomogeneous, and restricted trail, the current forms a closed loop). Setting as above $\theta = 90^\circ$ and taking a typical scale along x as $\Delta x = [4\psi Dt / (1+\psi)]^{1/2}$ and $N^{\text{ss}} \sim N_{\text{max}}$, according to Ampere's law, Eq. (88b), we estimate the typical magnetic field disturbance as

$$\delta B \sim \frac{2e\mu_0\Omega_e D}{\nu_{en}} \left(\frac{\psi}{1+\psi} \right) N_{\text{max}} = \frac{2\mu_0(T_e + T_i)}{(1+\psi)B_0} N_{\text{max}}, \quad (89)$$

where in the last equality we used the definitions of D , Eq. (11), and ψ , Eq. (2). The relative magnetic field disturbance is

$$\frac{\delta B}{B_0} \sim \frac{\beta_0 N_{\text{max}}}{(1+\psi)N_0}, \quad (90)$$

where β_0 is the ratio of the undisturbed total plasma pressure, $N_0(T_e + T_i)$, to the magnetic pressure, $B_0^2/2\mu_0$,

$$\beta_0 \approx 1.39 \times 10^{-6} \left(\frac{N_0}{10^{11} \text{m}^{-3}} \right) \left(\frac{T_e + T_i}{1000 \text{K}} \right) \left(\frac{0.5 \times 10^{-4} \text{T}}{B_0} \right)^2.$$

In the E-region ionosphere, $N_0 \simeq (10^9\text{--}10^{11}) \text{m}^{-3}$, $T_e \simeq T_i \simeq 300 \text{K}$, $B_0 \simeq (0.25\text{--}0.6) \times 10^{-4} \text{T}$, so that the relative disturbance of the magnetic field is small, unless the plasma trail is extremely dense, $N_{\text{max}}/N_0 \gtrsim 10^6\text{--}10^8$.

To estimate the contribution of the induction component into the total electric field, we can estimate the ratio of $|\nabla \times \mathbf{E}|$ to $|\nabla \cdot \mathbf{E}| \gtrsim (T_e + T_i)/e(\Delta x)^2$. According to Eqs. (88a) and (89), after simple algebra we obtain

$$\left| \frac{\nabla \times \mathbf{E}}{\nabla \cdot \mathbf{E}} \right| \lesssim \frac{4\Theta_0 \sqrt{\psi}}{(1+\psi)^2} \left(\frac{\delta B}{B_0} \right). \quad (91)$$

This ratio has an additional factor in front of $\delta B/B_0$, which is always small since according to Eq. (6), $4\Theta_0 \sqrt{\psi}/(1+\psi)^2 \leq 0.325\Theta_0 \simeq 0.44 \times 10^{-2}$. Because $\delta B/B_0$ in the regular meteor trail is small, the induction electric field proves to be even smaller. This justifies our initial assumption that the total electric field is nearly curl-free, $\mathbf{E} = -\nabla\phi$.

C. Dynamics of electric field and plasma instabilities

The ambipolar electric field associated with trail diffusion may drive plasma instabilities responsible for observable non-specular radar echoes. In this Section, we will make simple estimates of the driving field and instability threshold.

The driving field is determined by the total external force acting on electrons, $\mathbf{E}_{\text{res}} = -(T_e + T_i)\nabla\phi_{\text{res}}$, where ϕ_{res} is the residual potential defined by Eq. (4). Equations (82) to (84) give approximate analytical expressions for the residual potential if the magnetic field and the meteor trail axis are mutually orthogonal. These expressions depend upon the dimensionless parameter $\rho(t)$ given by Eq. (79) in terms of the effective rate γ , Eq. (26). The latter parameter is proportional to

an effective trail-background interaction cross-section $\sigma_{\text{eff}} \equiv N_{\text{lin}}/N_0$. After the critical time given by Eq. (66), the diffusion process becomes more isotropic and the residual potential decreases drastically. The critical time t_{cr} varies depending upon the ionospheric conditions and meteor parameters. Nighttime conditions with low N_0 and given N_{lin} are equivalent to daytime conditions with much larger N_0 and the proportionally increased column line density N_{lin} . For example, assuming equatorial day-time ionosphere, $N_0 \sim 10^{11} \text{m}^{-3}$, and a typical linear trail density, $N_{\text{lin}} \sim 10^{14} \text{m}^{-1}$ [1, 2], we obtain a critical time of tens of milliseconds. For mid- or high latitudes, night-time conditions, $N_0 \sim 10^9 \text{m}^{-3}$, and $N_{\text{lin}} \gtrsim 10^{15} \text{m}^{-1}$ (or faster and/or bigger meteoroids), we obtain that the critical time may reach tens of seconds.

The strongest electric field occurs in the early diffusion stage, $\rho \ll 1$, and at the edge of the nearly parabolic region of the potential, Eq. (35). Using Eqs. (36), (46), and Eq. (24), we obtain the maximum value of the residual electric field, $|E_x^{\text{max}}| \simeq [D\gamma \ln(1/\rho)/\rho]^{1/2} m_i \nu_{in}/e(1+\psi)$, where the diffusion coefficient D is defined by Eq. (11). In the later stage of trail diffusion when $\rho \gg 1$, Eq. (27) gives $[\partial_\eta \varphi(\eta)]^{\text{max}} \simeq 0.7/\rho$, ignoring the adjustment of ρ described in Sect. VD. In the original variables, we obtain $|E_x^{\text{max}}| \simeq 0.35(D\gamma/\rho)^{1/2} m_i \nu_{in}/e(1+\psi)\rho$. Interpolating between these limiting expressions, we can write a simple formula,

$$|E_x^{\text{max}}| \simeq \frac{m_i \nu_{in}}{e(1+\psi)} \left[\frac{D\gamma}{2\rho} \ln \left(1 + \frac{0.3}{\rho^2} \right) \right]^{1/2}, \quad (92)$$

roughly valid in the entire domain of ρ .

Now we estimate the Farley-Buneman (FB) instability criterion [26, 27]. For a homogeneous plasma, the simplest FB instability criterion, obtained using the two-fluid plasma model for sufficiently long-wavelength waves, is given by $|\mathbf{V}_0| > (1+\psi)C_s$ [28], where $\mathbf{V}_0 = \mathbf{E}_{\text{res}} \times \mathbf{B}_0/B_0^2$ is the $\mathbf{E}_{\text{res}} \times \mathbf{B}_0$ drift velocity and $C_s \equiv [(T_e + T_i)/m_i]^{1/2} = (D\nu_{in})^{1/2}$ is the ion-acoustic speed. Applying this criterion to the maximum field given by Eq. (92), expressing the corresponding drift speed as $|\mathbf{V}_0| = e|E_x^{\text{max}}|/m_i\Omega_i$, and using Eqs. (2) and (6), we write the FB instability criterion as $|E_x^{\text{max}}| > (1+\psi)(D\nu_{in})^{1/2} m_i \Omega_i/e$. Expressing E_x^{max} in N_{lin} , we reduce the FB instability criterion to

$$\frac{1}{\rho} \ln \left(1 + \frac{0.3}{\rho^2} \right) > P, \quad (93)$$

where

$$P = \frac{\Theta_0 (1+\psi)^{9/2} (eB_0)^2 N_{\text{lin}}}{\pi (T_e + T_i) m_i N_0} \approx 0.4 (1+\psi)^{9/2} \times \left(\frac{1000 \text{K}}{T_e + T_i} \right) \left(\frac{B_0}{0.5 \times 10^{-4} \text{T}} \right)^2 \left(\frac{N_{\text{lin}}}{10^{14} \text{m}^{-1}} \right) \left(\frac{10^{11} \text{m}^{-3}}{N_0} \right). \quad (94)$$

If this criterion is satisfied when the trail initially forms, then the instability starts generating plasma irregularities. If the instability persists for the sufficient time, then turbulence will develop and partially saturate through nonlinear processes.

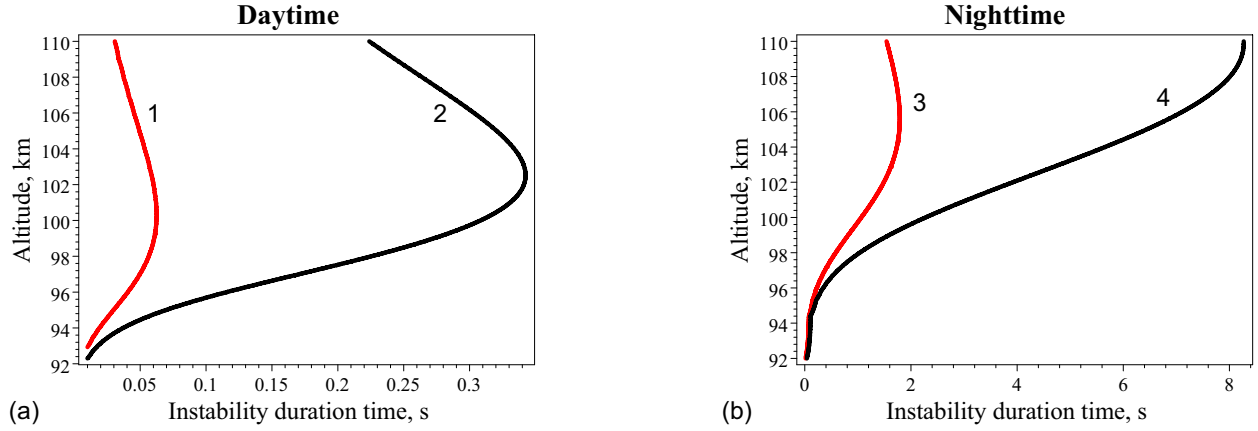


FIG. 13: Altitudinal dependence of FB instability duration t_{FB} for the equatorial E region during (a) daytime ($N_0 = 10^{11} \text{ m}^{-3}$), where curve 1 is for $N_{\text{lin}} = 10^{14} \text{ m}^{-1}$ and curve 2 is for $N_{\text{lin}} = 10^{15} \text{ m}^{-1}$, and (b) nighttime ($N_0 = 10^9 \text{ m}^{-3}$), where curve 3 is for $N_{\text{lin}} = 10^{14} \text{ m}^{-1}$ and curve 4 is for $N_{\text{lin}} = 10^{15} \text{ m}^{-1}$. Curves 1, 2, 3, and 4 correspond to $\sigma_{\text{eff}} = 10^3, 10^4, 10^5$, and 10^6 m^2 , respectively.

Because $\rho(t)$ monotonically increases with time, see Eq. (63), then at some moment, $t = t_{\text{FB}}$, the two sides of Eq. (93) become equal. At this moment, the linear growth of the FB instability starts being replaced by linear damping and irregularities will diffuse away. At $t < t_{\text{FB}}$, the linear FB instability sustain plasma turbulence at a certain level, while at $t > t_{\text{FB}}$ there is no more free energy to sustain the turbulence, so that irregularities will quickly disappear.

The instability duration t_{FB} depends critically upon the altitudinal parameter ψ and the effective trail-background interaction cross-section $\sigma_{\text{eff}} \equiv N_{\text{lin}}/N_0$. Due to this, the nighttime conditions with low N_0 will produce longer lived meteor trail than will the daytime conditions. Figure 13 shows the altitude dependence of the instability duration t_{FB} for several constant σ_{eff} during daytime and nighttime conditions. Notice clear peaks of t_{FB} at some intermediate altitudes which increase with σ_{eff} . The non-specular echo boundary for a given trail, like that in Fig. 1, should roughly follow the altitude dependence of t_{FB} . However, because column plasma density varies along the meteor trail and due to other inhomogeneities, we expect more variability than this model predicts. Measurements of the evolution of the trail echoes, in combination with other observations, should enable us to retrieve useful information about meteors, ionosphere and atmosphere. Implementation of this procedure requires better models of instability generation than that used above, as well as models of ablation and ionization to give improved estimates of N_{lin} [8, 12].

IX. SUMMARY

In this paper, we have described analytical theory and finite-element simulations of trail diffusion and fields for the mutually orthogonal trail axis and magnetic field. Unlike previous models, this theory includes both the trail and the background ionospheric plasma. This has two major effects: (1) a natural

restriction on the ambipolar electric field that otherwise would infinitely grow with distance from the trail and (2) a later-stage transition from sharply anisotropic (for $\psi \ll 1$) diffusion to nearly isotropic one. The former is important for plasma instabilities responsible for non-specular radar echoes, while the latter is important for interpreting specular radar echoes.

A key element of the present treatment is the introduction of the residual potential, ϕ_{res} , defined by Eq. (4). Its gradient describes the total force acting on electrons. Due to high electron mobility along the magnetic field \mathbf{B}_0 , the typical scale of ϕ_{res} spatial variations in this directions are much larger than that in the perpendicular direction, while the typical scales of trail density variations in both directions are comparable. This fact, which had not been realized in earlier simulations of meteor trail diffusion, requires setting the simulation box boundary along \mathbf{B}_0 far from the trail boundary and simultaneously resolving the two different scales parallel to \mathbf{B}_0 . In our simulations, we have overcome the computational difficulties by employing a finite-element software FlexPDE with the adaptive cell structure.

Based on the insight from simulations and using the large ratio of the electron and ion mobilities along the magnetic field, we have developed an approximate analytical approach. In this approach, the problems of trail diffusion and of spatial distribution of the residual potential are treated separately, while the coupling between the two is made via parameters and approximate solutions. In particular, Gaussian approximation of the trail peak has allowed us to treat the residual potential in terms of one parameter ρ . This parameter is proportional to the square of the trail peak dispersion, as described by Eq. (25), and monotonically grows with time. Due to high electron mobility along the magnetic field, the total force acting on electrons in this direction is much smaller than the corresponding components in other directions. For the particular case of mutually orthogonal trail axis and the magnetic field, this has allowed us to reduce the original 2D description to a 1D linear integrodifferential equation given

in two different forms by Eq. (23). This governing equation is for a residual potential in the near-trail zone and it has a unique solution depending upon ρ . The approximate solution of Eq. (23) depends on the range of ρ , as described in Sect. VB. Using this solution, we have obtained the approximate expression for $\rho(t)$, Eq. (63), which closes the entire description of trail diffusion and fields. Note that the near-trail potential, which is easily spread along the magnetic field, may create significant disturbances of the background plasma beyond the trail, as described in Sect. VD.

Comparison of analytical theory with simulations have demonstrated good agreement between the results with one exception. At a later stage of trail diffusion, the parameter ρ for the residual potential should be replaced by an adjusted parameter $\tilde{\rho}$ as described in Sect. VII. We have identified the nature of this deviation analytically in terms of the disturbances of the background plasma, but to quantitatively relate $\tilde{\rho}$ and ρ we have invoked simulations.

The analytical theory and simulations have allowed us to estimate the spatial distribution of the ambipolar electric field within and near the plasma trail. These fields are crucial for plasma instabilities responsible for generation of field-aligned electron density irregularities observed by high-power large-aperture (HPLA) radars as non-specular echoes. Measuring the characteristics of non-specular echoes and some other characteristics should allow one to retrieve an important information on the meteoroids and the surrounding atmosphere.

Acknowledgments

Work was supported by National Science Foundation Grants No. ATM-9986976, ATM-0332354, and ATM-0334906. Authors thank L. Dyrud and T. Lin for their help and fruitful discussions.

APPENDIX A: SELF-SIMILAR SOLUTION

In this Appendix, we obtain explicit expressions for the self-similar solution (SSS) proposed in the general form, but not found explicitly, by Jones [17]. In our notations, this solution (denoted below by superscript 'ss') follows the ansatz $n(\mathbf{r}, t) = n^{\text{ss}}(x, y, t)$ and $\phi_{\text{res}}(\mathbf{r}, t) = \phi_{\text{res}}^{\text{ss}}(x, y, t)$, where

$$n^{\text{ss}}(x, y, t) = \frac{C}{t} \exp\left(-\frac{A_{xx}x^2 + A_{yy}y^2 + A_{xy}xy}{4Dt}\right), \quad (\text{A1})$$

$$\phi_{\text{res}}^{\text{ss}}(x, y, t) = \frac{B_{xx}x^2 + B_{yy}y^2 + B_{xy}xy}{4Dt} + \text{const}, \quad (\text{A2})$$

with positive diagonal coefficients A_{ii} , B_{ii} and

$$A_{xx}A_{yy} > \frac{A_{xy}^2}{4}, \quad B_{xx}B_{yy} > \frac{B_{xy}^2}{4}. \quad (\text{A3})$$

This is the solution to Eq. (10) in an infinite and homogeneous neutral atmosphere with no background plasma, provided the

diffusion starts from an infinitely thin and dense plasma column with a given line density. The electron Hall velocities give rise to the non-diagonal coefficients, $A_{xy} = B_{xy}$. Inequalities given by Eq. (A3) mean that the contours of the constant density and the residual potential form ellipses in the xy -plane, whose major axes are rotated with respect to the x and y axes through a common angle χ determined by

$$\tan 2\chi = \frac{A_{xy}}{A_{xx} - A_{yy}} = \frac{B_{xy}}{B_{xx} - B_{yy}} \quad (\text{A4})$$

The constant C in (A1) is expressed in terms of the conserved linear density (along the z coordinate), N_{lin} , as

$$C = \frac{(4A_{xx}A_{yy} - A_{xy}^2)^{1/2} N_{\text{lin}}}{8\pi D N_0}. \quad (\text{A5})$$

For arbitrary electron and ion mobilities it is hard to obtain explicit analytical expressions for the coefficients A_{ij} and B_{ij} . However, under restrictions described by Eq. (12), to leading order accuracy with respect to the small parameters Q^{-1} , ψQ^{-1} , $(\psi Q)^{-1}$, we obtain

$$\begin{aligned} A_{xx} &= 1 + B_{xx}, & B_{xx} &= \frac{\sin^2 \theta}{\psi}, \\ A_{yy} &= 1 + B_{yy}, & B_{yy} &= \frac{1 + \cos^2 \theta}{Q} = \Theta_0^2 \left(\frac{1 + \cos^2 \theta}{\sin^2 \theta} \right), \end{aligned} \quad (\text{A6})$$

$$A_{xy} = B_{xy} = -\frac{2\mu}{Q} \frac{\sin^2 \theta}{\psi} = -\frac{2\Omega_i}{\nu_{in}} \cos \theta.$$

The non-diagonal coefficient, $A_{xy} = B_{xy}$, is always small compared to A_{xx} , and $A_{yy} \approx 1$, but not necessarily to B_{xx} and $B_{yy} \ll 1$. The rotation angle, Eq. (A4), is small $|\tan 2\chi| \approx 2\nu_{en} \cos \theta / (\Omega_e \sin^2 \theta)$. Because

$$\frac{A_{xy}^2}{4A_{xx}A_{yy}} \approx \frac{\mu^2}{Q^2} \frac{\sin^4 \theta}{\psi(\psi + \sin^2 \theta)} = \frac{\Theta_0^2 \cos^2 \theta}{\psi + \sin^2 \theta} \ll 1,$$

we have

$$C \approx \frac{N_{\text{lin}}}{4\pi D N_0} \left(1 + \frac{\sin^2 \theta}{\psi}\right)^{1/2}. \quad (\text{A7})$$

The residual potential is stretched along the coordinate y in accord with the qualitative discussion in Sect. II, which holds under condition

$$\theta^2 \gg \frac{\nu_{en}}{\Omega_e} = \Theta_0 \sqrt{\psi}. \quad (\text{A8})$$

This restriction due to the electron Hall velocity is stronger than that of Eq. (7a). For the trail strictly perpendicular to \mathbf{B} , $\cos \theta = 0$, $\mu = 0$, Hall velocity is directed along z and plays no role in 2D trail diffusion.

To the same accuracy, the particle fluxes are given by

$$\Gamma_{ex} = \Gamma_{ix} = \frac{x}{2t} n^{\text{ss}}(x, y, t), \quad \Gamma_{ey} = \Gamma_{iy} = \frac{y}{2t} n^{\text{ss}}(x, y, t),$$

$$\Gamma_{iz} = 0, \quad \Gamma_{ez} = -\frac{\Omega_e}{\nu_{en}} \frac{x \sin \theta}{2t} n^{ss}(x, y, t) \quad (\text{A9})$$

In the SSS, the flux components in both x and y directions are equal for electrons and ions. The only disparity is in the flux component along the z -axis due to electron Hall velocity. The net electric current is directed along the trail axis with the current density

$$j_z = \frac{e\Omega_e}{\nu_{en}} \left(\frac{x \sin \theta}{2t} \right) n^{ss}(x, y, t). \quad (\text{A10})$$

APPENDIX B: RESIDUAL POTENTIAL IN THE FAR ZONE

In this Appendix, we solve for ϕ_{res} in the far zone $|\zeta| \gg 1$, where $\zeta = y/(Dt)^{1/2}$ is a coordinate parallel to \mathbf{B}_0 . This zone is located well beyond the plasma trail. Neglecting plasma density disturbances allows us to reduce Eq. (15b) to the Laplace equation

$$\partial_{\xi\xi}\phi_{\text{res}} + \partial_{\zeta'\zeta'}\phi_{\text{res}} = 0, \quad (\text{B1})$$

where we have renormalized the variable ζ as $\zeta' = \alpha\zeta$ with

$$\alpha = \left(\frac{1 + \psi}{Q} \right)^{1/2} = \Theta_0 (1 + \psi)^{1/2} \ll 1. \quad (\text{B2})$$

In terms of ξ and ζ' , the near zone described in the following Appendix, reduces to a thin strip extended along ξ . Assuming that potential disturbances have typical scales of order unity with respect to both coordinates, we can approximate this strip by a cut in the ξ, ζ' -plane at $\zeta' = \pm 0$. Here the signs \pm mean infinitesimal offsets from zero to either positive or negative directions. Because of the mirror symmetry with respect to the ξ -axis, Eqs. (19b), we will consider only the positive half-space, $\zeta' > 0$.

The nearly constant value of the residual potential in the near zone represents a boundary condition for $\phi_{\text{res}}(\xi, \zeta')$ at the cut,

$$[\phi_{\text{res}}(\xi, \zeta')]_{\zeta'=\pm 0} \approx \phi_{\text{res}}^0(\xi). \quad (\text{B3})$$

Other boundary conditions are given by $\phi_{\text{res}}(\xi, \zeta') \rightarrow 0$ as $\xi, \zeta' \rightarrow \pm\infty$. The solution of Eq. (B1) with these boundary conditions (the Dirichlet problem for the upper half-space, $\zeta' > 0$) is given by

$$\begin{aligned} \phi_{\text{res}}(\xi, \zeta') &= \frac{\zeta'}{\pi} \int_{-\infty}^{\infty} \frac{\phi_{\text{res}}^0(\tau) d\tau}{(\tau - \xi)^2 + \zeta'^2} \\ &= \frac{\alpha\zeta}{\pi} \int_{-\infty}^{\infty} \frac{\phi_{\text{res}}^0(\tau) d\tau}{(\tau - \xi)^2 + \alpha^2\zeta^2} \end{aligned} \quad (\text{B4})$$

In particular, for $\xi^2 + \zeta'^2 \gg 1$, Eq. (B4) reduces to a 2D quadrupole,

$$\phi_{\text{res}}(\xi, \zeta') \approx \frac{C(\xi^2 - \zeta'^2)}{(\xi^2 + \zeta'^2)^2}. \quad (\text{B5})$$

In polar coordinates, r and θ are defined as $\xi = r \cos \theta$, $\zeta' = r \sin \theta$, the quadrupole potential is $\phi_{\text{res}}(r, \theta) \approx (C \cos 2\theta)/r^2$, while the electric field lines of force are determined by $(\sin 2\theta)/r^2 = \text{const.}$ Here the constant C is determined by the distribution of $\phi_{\text{res}}(\xi)$ along the cut $\zeta = 0$, as discussed in Appendix D.

Now we obtain general relations which follow from Laplace Eq. (B1) and will be used in Appendix C to derive a closed equation for $\phi_{\text{res}}^0(\xi)$ when combined with the residual potential in the near zone. Introducing a complex coordinate,

$$Z = \xi + i\zeta', \quad (\text{B6})$$

we consider $\zeta' > 0$ as a complex half-plane and introduce a complex potential,

$$\Psi(Z) = \phi_{\text{res}}(\xi, \zeta') + iW(\xi, \zeta'), \quad (\text{B7})$$

where the function $W(\xi, \zeta)$ also satisfies Laplace Eq. (B1). This is an analytic function of the complex coordinate Z with ϕ_{res} and W related by the Cauchy-Riemann equations,

$$\partial_{\xi}\phi_{\text{res}} = \partial_{\zeta'}W, \quad \partial_{\zeta'}\phi_{\text{res}} = -\partial_{\xi}W. \quad (\text{B8})$$

At the cut, $\zeta' = +0$, we denote $w^0(\xi) \equiv W(\xi, +0)$, so that from Eq. (B8) we have

$$\partial_{\xi}\phi_{\text{res}}^0 = \partial_{\zeta'}W|_{\zeta'=+0}, \quad \partial_{\zeta'}\phi_{\text{res}}|_{\zeta'=+0} = -\partial_{\xi}w^0. \quad (\text{B9})$$

According to the mirror symmetry, Eq. (19b), the function $\phi_{\text{res}}^0(\xi)$ is even, while $w^0(\xi)$ is odd,

$$\phi_{\text{res}}^0(\xi) = \phi_{\text{res}}^0(-\xi), \quad w^0(\xi) = -w^0(-\xi). \quad (\text{B10})$$

At large Z , the residual potential $\phi_{\text{res}} \propto 1/|Z|^2$ decreases faster than $1/|Z|$ as $|Z| \rightarrow \infty$. According to the Cauchy-Goursat theorem, $\oint_C \Psi(Z) dZ = 0$, so that we have

$$\int_{-\infty}^{\infty} \phi_{\text{res}}^0(\xi) d\xi = 0, \quad \int_{-\infty}^{\infty} w^0(\xi) d\xi = 0. \quad (\text{B11})$$

While the integral relation for $w^0(\xi)$ is trivial because w^0 is odd, the integral relation for the even function $\phi_{\text{res}}^0(\xi)$ represents an important constraint.

Now we proceed with the complex potential $\Psi(Z)$. In the upper half-plane, we consider the continuous contour C , which includes the axis $\zeta' = +0$ with an infinitesimal half-circle around $Z' = \xi + i0$, and the infinite half-circle, $|Z| \rightarrow \infty$. Because Ψ is an analytic function and the pole $Z = Z'$ is beyond the area closed by this contour, the residue theorem yields $\oint_C \Psi(Z)/(Z - Z') dZ = 0$, or

$$\mathcal{P} \int_{-\infty}^{\infty} \frac{\Psi(\tau)}{\tau - \xi} d\tau = i\pi\Psi(\xi), \quad (\text{B12})$$

where \mathcal{P} denotes the principal value of the integral along the real axis. Separating in Eq. (B12) the real and imaginary part, we obtain

$$\phi_{\text{res}}^0(\xi) = \frac{1}{\pi} \mathcal{P} \int_{-\infty}^{\infty} \frac{w^0(\tau)}{\tau - \xi} d\tau, \quad (\text{B13a})$$

$$w^0(\xi) = -\frac{1}{\pi} \mathcal{P} \int_{-\infty}^{\infty} \frac{\phi_{\text{res}}^0(\tau)}{\tau - \xi} d\tau. \quad (\text{B13b})$$

These equations are equivalent to the well-known Kramers-Kronig dispersion relations in optics, plasma physics, etc., which are derived in the same way. Applied to an arbitrary function $\phi_{\text{res}}^0(\xi)$ [or $w^0(\xi)$], Eq. (B13) is also known as the Hilbert transform [29, 30]. Equation (B13) will be applied in Appendix C and Sect. V B.

APPENDIX C: NEAR-ZONE POTENTIAL

In this Appendix, using the results of Appendix B, we derive the governing equation for the residual potential in the near zone, $|\zeta| \ll 1/\alpha$, where $\alpha = \Theta_0(1 + \psi)^{1/2} \ll 1$ is defined by Eq. (B2). To obtain a closed equation for $\phi_{\text{res}}(\xi)$, we write Eq. (15) for $\mu = 0$ in a conservative form as

$$\partial_t(t\Delta n) - \frac{\partial_\xi(\xi\Delta n) + \partial_\zeta(\zeta\Delta n)}{2} - \nabla^2\Delta n - \nabla \cdot [(1 + \Delta n)\nabla\phi_{\text{res}}] = 0, \quad (\text{C1a})$$

$$\partial_\xi[(1 + \Delta n)\partial_\xi\phi_{\text{res}}] + \frac{1}{\alpha^2}\partial_\zeta[(1 + \Delta n)\partial_\zeta\phi_{\text{res}}] + \frac{\nabla^2\Delta n}{1 + \psi} = 0, \quad (\text{C1b})$$

where $\Delta n \equiv \Delta N/N_0$ is the total density disturbance which includes both the plasma trail and the background plasma disturbance. We assume that the major density disturbances are concentrated within the near zone, $\zeta \ll 1/\alpha$, where the residual potential is only weakly ζ -dependent. In this zone, which overlaps with the far zone $\zeta \gg 1$, we represent the residual potential as

$$\phi_{\text{res}}(\xi, \zeta) = \phi_{\text{res}}^{\text{far}}(\xi, \zeta) + \delta\phi(\xi, \zeta), \quad |\delta\phi| \ll |\phi_{\text{res}}^{\text{far}}|, \quad (\text{C2})$$

where $\phi_{\text{res}}^{\text{far}}(\xi, \zeta)$ is the component in the far zone and therefore satisfies the Laplace equation described in Appendix B. Because most of the potential changes occur in the background plasma (far zone), our assumption $|\delta\phi| \ll |\phi_{\text{res}}^{\text{far}}|$ is well justified as can be seen in the example solution shown in Fig. 5. The function $\phi_{\text{res}}^{\text{far}}(\xi, \zeta)$ varies along ζ with a large scale-length typical for the far zone, so that within the near-zone it varies approximately linearly

$$\phi_{\text{res}}^{\text{far}}(\xi, \zeta) \approx \phi_{\text{res}}^{\text{far}}(\xi, 0) + \zeta\partial_\zeta\phi_{\text{res}}^{\text{far}}(\xi), \quad (\text{C3})$$

where $|\partial_\zeta\phi_{\text{res}}^{\text{far}}| \ll |\phi_{\text{res}}^{\text{far}}(\xi, 0)|$, with the derivative $\partial_\zeta\phi_{\text{res}}^{\text{far}}$ remaining nearly ζ -independent across a transitional zone between the near and far zones as seen in Fig. 5. The perturbation $\delta\phi(\xi, \zeta)$, associated with strong density disturbances in the near zone, is relatively small, but its ζ -derivative is not small compared to $\partial_\zeta\phi_{\text{res}}^{\text{far}}$. Furthermore, it is this perturbation that provides a smooth transition from the zero ζ derivative of $\phi_{\text{res}}(\xi, \zeta)$ at the symmetry center, $\partial_\zeta\phi_{\text{res}}|_{\zeta=0} = 0$,

$$\partial_\zeta\delta\phi_{\text{res}}|_{\zeta=0} = -\partial_\zeta\phi_{\text{res}}^{\text{far}}, \quad (\text{C4})$$

to the finite derivatives $\partial_\zeta\phi_{\text{res}} \approx \partial_\zeta\phi_{\text{res}}^{\text{far}}$ in the far zone where $\delta\phi(\xi, \zeta)$ gradually disappears. Now we subtract from

Eq. (C1b) the Laplace equation for $\phi_{\text{res}}^{\text{far}}$ and integrate over ζ from 0 to $\zeta = \zeta_1$, where $\zeta_1 \ll \alpha^{-1}$ is located in the transitional zone where both $\delta\phi$ and $\partial_\zeta\delta\phi$ are zero. Also, at $\zeta = \zeta_1$ we neglect the density disturbances Δn and the perturbations $\delta\phi_{\text{res}}$ with their derivatives, except in the term $\propto 1/\alpha^2$. We will also ignore within the range $|\zeta| < \zeta_1$ all density disturbances other than the trail plasma itself. (This introduces some error which we correct in Sect. V D 2 and Appendix F.) The range $|\zeta| < \zeta_1$ includes practically the entire trail, so that we can extend the upper limit of all density integrals to infinity. As a result, using Eq. (C4), we obtain

$$\partial_\xi(\Delta N_{\zeta_1}\partial_\xi\phi_{\text{res}}^{\text{far}}) + \frac{1}{\alpha^2}\partial_\zeta\phi_{\text{res}}^{\text{far}} + \left(\frac{1}{1 + \psi}\right)\partial_{\xi\xi}^2(\Delta N_{\zeta_1}) = 0. \quad (\text{C5})$$

Here

$$\Delta N_{\zeta_1}(\xi) \equiv \int_0^{\zeta_1}\Delta n d\zeta \approx \Delta N_{\text{Trail}}(\xi) \equiv \int_0^\infty\Delta n_{\text{Trail}} d\zeta. \quad (\text{C6})$$

where Δn_{Trail} is the part of the total density disturbance associated only with the trail plasma.

To good accuracy, the trail plasma distribution is described by a Gaussian distribution, see Sect. IV and V C,

$$\Delta n_{\text{Trail}}(\xi, \zeta, t) = \frac{n_0 t_0}{t} \sqrt{\frac{q_0}{q(t)}} \exp\left[-\left(\frac{\xi^2}{4q(t)} + \frac{\zeta^2}{4}\right)\right], \quad (\text{C7})$$

where $q_0 = \psi/(1 + \psi)$ and $q(t)$ gradually varies between q_0 and 1. Because $\phi_{\text{res}}^{\text{far}}$ is the far-zone potential, we apply Eq. (B9), $\partial_\zeta\phi_{\text{res}}^{\text{far}} = -\alpha\partial_\xi w^0(\xi)$. Bearing in mind Eq. (C3), in Eq. (C5) we can eliminate all ζ -dependence, $\phi_{\text{res}}^{\text{far}}(\xi, \zeta) \approx \phi_{\text{res}}^0(\xi) \equiv \phi_{\text{res}}^{\text{far}}(\xi, 0)$, and obtain

$$\partial_\xi(\Delta N_{\zeta_1}\partial_\xi\phi_{\text{res}}^0) - \frac{1}{\alpha}\partial_\xi w^0 + \left(\frac{1}{1 + \psi}\right)\partial_{\xi\xi}^2\Delta N_{\zeta_1} = 0, \quad (\text{C8})$$

where

$$\Delta N_{\zeta_1}(\xi) \approx \frac{\sqrt{\pi}n_0 t_0}{t} \sqrt{\frac{q_0}{q(t)}} \exp\left(-\frac{\xi^2}{4q(t)}\right). \quad (\text{C9})$$

Integrating Eq. (C8) with the boundary condition $w^0 \rightarrow 0$ at $|\xi| \rightarrow \infty$ and expressing w^0 in terms of ϕ_{res}^0 according to (B13b), we obtain

$$\partial_\xi\phi_{\text{res}}^0 + \frac{1}{\pi\alpha\Delta N_{\zeta_1}}\mathcal{P}\int_{-\infty}^\infty\frac{\phi_{\text{res}}^0(\chi)}{\chi - \xi}d\chi = \frac{\xi}{2(1 + \psi)q(t)}. \quad (\text{C10})$$

Renormalizing the potential and coordinate as follows,

$$\varphi = 2(1 + \psi)\phi_{\text{res}}^0, \quad \xi = \sqrt{q}\eta, \quad (\text{C11})$$

we arrive at an integrodifferential equation

$$\partial_\eta\varphi + \frac{2\rho e^{n^2/4}}{\pi^{3/2}}\mathcal{P}\int_{-\infty}^\infty\frac{\varphi(\tau)}{\tau - \eta}d\tau = \eta, \quad (\text{C12})$$

which depends only upon one dimensionless parameter

$$\rho(t) = \frac{\sqrt{\pi q(t)}}{2\alpha\Delta N_{\zeta_1}(0)} = \gamma q(t)t, \quad \gamma = \frac{1}{2\Theta_0 n_0 t_0 \sqrt{\psi}} = \frac{\rho_0}{t_0 q_0}. \quad (\text{C13})$$

Here

$$\rho_0 \equiv \rho(t_0) = \frac{\sqrt{\psi}}{2\Theta_0 n_0 (1 + \psi)}. \quad (\text{C14})$$

Multiplying Eq. (C12) by $\exp(-\eta^2/4)$, applying the Hilbert transform, Eq. (B13), and using the identity

$$\mathcal{P} \int_{-\infty}^{\infty} \frac{1}{\tau - \eta} \left(\mathcal{P} \int_{-\infty}^{\infty} \frac{\varphi(\chi)}{\chi - \tau} d\chi \right) d\tau = -\pi^2 \varphi(\eta),$$

we arrive at a different form of integrodifferential Eq. (C12),

$$\rho \varphi(\eta) - \frac{1}{2\sqrt{\pi}} \mathcal{P} \int_{-\infty}^{\infty} \frac{\partial_{\tau} \varphi(\tau)}{\tau - \eta} e^{-\tau^2/4} d\tau = S(\eta). \quad (\text{C15})$$

The function $S(\eta)$ in the RHS of Eq. (C15) stems from the integration

$$S(\eta) = -\frac{1}{2\sqrt{\pi}} \mathcal{P} \int_{-\infty}^{\infty} \frac{\tau e^{-\tau^2/4}}{\tau - \eta} d\tau \quad (\text{C16})$$

and can be recast as

$$\begin{aligned} S(\eta) &= \eta e^{-\eta^2/4} \int_0^{\eta/2} e^{\tau^2} d\tau - 1 \\ &= -\left[\frac{i\sqrt{\pi}}{2} \eta e^{-\eta^2/4} \operatorname{erf}\left(\frac{i\eta}{2}\right) + 1 \right], \end{aligned} \quad (\text{C17})$$

where $\operatorname{erf}(x)$ denotes the standard error-function.

Now we discuss some properties of the function $S(\eta)$, which will be used in Sect. V B and others. Firstly, we observe that Eq. (C16) shows that $S(\eta)$ and $(\sqrt{\pi}/2)\eta \exp(-\eta^2/4)$ form a Hilbert transform pair, Eqs. (B13a,b), so that

$$\mathcal{P} \int_{-\infty}^{\infty} \frac{S(\tau)}{\tau - \eta} d\tau = \frac{\pi^{3/2}}{2} \eta \exp\left(-\frac{\eta^2}{4}\right). \quad (\text{C18})$$

Considering the double integral

$$K = \int_{-\infty}^{\infty} d\eta \mathcal{P} \int_{-\infty}^{\infty} \frac{F(y)}{y - \eta} dy,$$

with an arbitrary integrable function $F(y)$ and changing the order of integration, we verify that $K = 0$. Applying this to Eq. (C16), we conclude that the even function $S(\eta)$ obeys

$$\int_0^{\infty} S(\eta) d\eta = 0. \quad (\text{C19})$$

The function $S(\eta)$ has important power-series approximations at sufficiently small and large values of $|\eta|$. The function $S(\eta)$ can be represented as an infinite Taylor series,

$$\begin{aligned} S(\eta) &= -1 + \frac{1}{2} \sum_{n=1}^{\infty} (-1)^{n-1} \frac{\eta^{2n} (n-1)!}{(2n-1)!} \\ &= -1 + \frac{\eta^2}{2} - \frac{\eta^4}{2 \times 6} + \frac{\eta^6}{2 \times 6 \times 10} - \dots \end{aligned} \quad (\text{C20})$$

which is convergent for all values of η . A truncated series with a few first terms approximates the function at $|\eta| < 2$ well. At $|\eta| > 4$, the function $S(\eta)$ can be approximated well by an asymptotic series,

$$S(\eta) \approx 2 \sum_{n=1}^{n_{\max}} \frac{(2n-1)!}{(n-1)! \eta^{2n}} = \frac{2}{\eta^2} + \frac{2 \times 6}{\eta^4} + \frac{2 \times 6 \times 10}{\eta^6} + \dots \quad (\text{C21})$$

Unlike the Taylor series, this asymptotic series is divergent, so that the total number of terms n_{\max} should not be too large.

To conclude this Appendix, we calculate the integral

$$J(\eta) = -\frac{1}{2\sqrt{\pi}} \mathcal{P} \int_{-\infty}^{\infty} \frac{\partial_{\tau} S(\tau)}{\tau - \eta} e^{-\tau^2/4} d\tau, \quad (\text{C22})$$

needed to obtain the first-order correction of the later-stage residual potential in Sect. V B 1. Exact integration yields

$$\begin{aligned} J(\eta) &= \left(1 - \frac{\eta^2}{2}\right) e^{-\eta^2/2} \left[\frac{1}{2} \left(\int_0^{\eta/2} e^{y^2} dy \right)^2 - \frac{\pi}{8} \right] \\ &+ \frac{1}{2} \left(\eta e^{-\eta^2/4} \int_0^{\eta/2} e^{y^2} dy - \frac{1}{2} \right). \end{aligned} \quad (\text{C23})$$

The function $J(\eta)$ looks qualitatively as $S(\eta)$ and to a good accuracy can be approximated by a simpler expression

$$J(\eta) \approx \tilde{J}(\eta) = l S(p\eta), \quad (\text{C24})$$

where the constants l and p are given by

$$l = \frac{\pi + 2}{8} \approx 0.643, \quad (\text{C25a})$$

$$p = \left(\frac{3 + \pi}{1 + \pi/2} \right)^{1/2} \approx 1.546. \quad (\text{C25b})$$

We have chosen these constants to provide the best parabolic fit between $J(\eta)$ and $\tilde{J}(\eta)$ at $\eta = 0$. The biggest difference between the exact and approximate expressions for $J(\eta)$ is near the maxima of $J(\eta)$ ($|\eta| \approx 2$), where it reaches about 0.016 (less than 10%, see Fig. 8). In all other locations, the functions $J(\eta)$ and $\tilde{J}(\eta)$ are much closer to each other.

APPENDIX D: PROPERTIES OF RESIDUAL POTENTIAL

In this Appendix, we discuss general properties of solutions of Eq. (23). The solution of $\varphi(x)$ has the following important property,

$$\int_0^{\infty} \varphi(x) dx = 0, \quad (\text{D1})$$

which follows from general properties of analytic functions [see Eq. (B11)] and symmetry (19b), and is necessary for the consistency of Cauchy type integrodifferential Eq. (23). We may rewrite this relation in terms of the x component of the

electric field $E_x = -\partial_x \varphi$. Expressing the residual potential as $\varphi(x) = \int_x^\infty E_x d\tilde{x}$, substituting this in Eq. (D1), and changing the order of integration, we obtain

$$\int_0^\infty E_x(x) x dx = 0. \quad (\text{D2})$$

In addition, Eqs. (23a,b) impose restrictions on possible asymptotic behavior of the residual potential at large distances. For $|\eta| \gg 1$, we expect the function $\varphi(\eta)$ to behave as

$$\varphi(\eta) \simeq \sum_{k=1}^{k_{\max}} \frac{C_k}{\eta^{2k}}, \quad (\text{D3})$$

which corresponds to the expansion of the electric potential in multipoles. Note that the lowest-order coefficient C_1 , in accord with Eq. (C11), relates to the quadrupole coefficient C in Eq. (B5) as $C_1 = 2(1 + \psi)C$. The maximum value of k , k_{\max} , is determined by η (the asymptotic series may diverge as $k \rightarrow \infty$). The electric field proportional to $\partial_\eta \varphi$ tends to zero as $|\eta| \rightarrow \infty$. This means that the RHS of Eq. (23a), i.e., the term η , should asymptotically match the integral term in the LHS of Eq. (23a). The exponentially growing factor in front of the principal value integral requires the integral to decrease as $|\eta| \rightarrow \infty$ faster than $|\eta|^{-n}$ with positive n . Analyzing the asymptotic behavior of the integral, one can obtain the following restriction,

$$\int_{-\infty}^\infty \left(\varphi(\eta) - \sum_{k=1}^m \frac{C_k}{\eta^{2k}} \right) \eta^{2m} d\eta = 0, \quad (\text{D4})$$

valid for any positive integer m [in the case of $m = 0$, we obtain Eq. (D1)]. From Eq. (D4) it follows that the residual potential cannot be an exponentially decreasing function of η as $|\eta| \rightarrow \infty$, but must have a power-law asymptotic behavior (as required by the multipole expansion). Indeed, all coefficients C_n cannot equal zero because no non-zero $\varphi(x)$ could satisfy Eq. (D4) for all positive integer m .

The self-similar solution (SSS) for the residual potential, defined in Appendix A (to the accuracy of an arbitrary constant), in variables defined by Eq. (C11) can be written as $\varphi(0) + \eta^2/2$. Introducing the difference between the actual potential $\varphi(\eta)$ and the SSS,

$$\delta\varphi(\eta) \equiv \varphi(\eta) - \varphi(0) - \frac{\eta^2}{2}, \quad (\text{D5})$$

we rewrite Eqs. (23) as a Hilbert transform pair:

$$\partial_\eta \delta\varphi(\eta) e^{-\frac{\eta^2}{4}} = -\frac{2\rho}{\pi^{3/2}} \mathcal{P} \int_{-\infty}^\infty \frac{\varphi(\tau)}{\tau - \eta} d\tau. \quad (\text{D6a})$$

$$\rho\varphi(\eta) = \frac{1}{2\sqrt{\pi}} \mathcal{P} \int_{-\infty}^\infty \frac{\partial_\tau \delta\varphi(\tau)}{\tau - \eta} e^{-\frac{\tau^2}{4}} d\tau, \quad (\text{D6b})$$

We expect $\delta\varphi(\eta) \approx -\lambda\eta^2$ as $|\eta| \ll 1$ with a positive constant λ and $\delta\varphi(\eta) \approx -\eta^2/2$ as $|\eta| \gg 1$. Considering the limits of

small and large values of $|\eta|$, we obtain integral relations

$$\begin{aligned} \varphi(0) &= \frac{1}{\sqrt{\pi}\rho} \int_0^\infty \frac{\partial_\tau \delta\varphi(\tau)}{\tau} e^{-\frac{\tau^2}{4}} d\tau, \\ \frac{d\varphi(\eta)}{d(\eta^2)} \Big|_{\eta=0} &= \frac{1}{\sqrt{\pi}\rho} \int_0^\infty \frac{1}{\tau} \partial_\tau \left(\frac{\partial_\tau \delta\varphi(\tau)}{\tau} e^{-\frac{\tau^2}{4}} \right) d\tau, \\ \lim_{|\eta| \rightarrow \infty} [\varphi(\eta)\eta^2] &\equiv 2(1 + \psi) C_1 \\ &= -\frac{1}{\sqrt{\pi}\rho} \int_0^\infty \partial_\tau \delta\varphi(\tau) \tau e^{-\frac{\tau^2}{4}} d\tau, \end{aligned} \quad (\text{D7})$$

which describe the parabolic behavior of the residual potential near its minimum and express the highest-order multipole coefficient in terms of deviation from the self-similar potential. Equations (D1), (D4), (D7), as well as the exact relations obtained in the following Appendix, can be used for checking the solution.

APPENDIX E: DENSITY DISTURBANCE INTEGRALS

In this Appendix, we derive an important exact property of density disturbance integrals (DDIs), which have been applied for monitoring the simulation accuracy, see Sect. IV and VII. We define the two DDIs by integrating parallel and perpendicular to \mathbf{B}_0 ,

$$\Delta N_\zeta(\xi, t) = \int_{-\infty}^\infty \Delta n(\xi, \zeta, t) d\zeta, \quad (\text{E1a})$$

$$\Delta N_\xi(\zeta, t) = \int_{-\infty}^\infty \Delta n(\xi, \zeta, t) d\xi, \quad (\text{E1b})$$

where Δn include both the plasma trail density and disturbances of the background plasma. If we solve Eq. (15) with the self-similar solution (SSS) as the initial condition then the DDIs multiplied by t , for all coordinates ζ or ξ , are strictly conserved and equal to those for the SSS, even though the SSS is, in general, invalid.

To prove this and obtain the explicit analytical expressions for the DDIs, we start from Eqs. (C1a,b). Adding them, we eliminate ξ -derivatives of ϕ_{res} ,

$$\begin{aligned} \partial_t (t\Delta n) - \frac{\partial_\xi (\xi \Delta n) + \partial_\zeta (\zeta \Delta n)}{2} - \frac{\psi \nabla^2 \Delta n}{1 + \psi} \\ + \frac{1 - \alpha^2}{\alpha^2} \partial_\zeta [(1 + \Delta n) \partial_\zeta \phi_{\text{res}}] = 0. \end{aligned} \quad (\text{E2})$$

Because both the density disturbance and the potential go to zero at infinity, we integrate this equation along the coordinate ζ from $-\infty$ to ∞ and obtain

$$\partial_t (t\Delta N_\zeta) - \partial_\xi \left[\left(\frac{\xi}{2} + \frac{\psi}{1 + \psi} \partial_\xi \right) \Delta N_\zeta \right] = 0. \quad (\text{E3})$$

Similarly, multiplying Eq. (C1b) by α^2 and adding with (C1a), we eliminate ζ -derivatives of ϕ_{res} . After the integration over ξ we obtain

$$\partial_t (t\Delta N_\xi) = \partial_\zeta \left[\left(\frac{\zeta}{2} + \partial_\zeta \right) \Delta N_\xi \right]. \quad (\text{E4})$$

If we use the SSS as the initial condition at $t = t_0$ in Eqs. (E3) and (E4) then $[\partial_t (t\Delta N_\xi)]_{t=t_0} = 0$ and $[\partial_t (t\Delta N_\zeta)]_{t=t_0} = 0$. The unique solutions of Eqs. (E3) and (E4) will keep these relations in their self-similar form,

$$\Delta N_\zeta(\xi, t) = \frac{2C}{t} \sqrt{\pi} \exp\left[-\left(\frac{1+\psi}{\psi}\right) \frac{\xi^2}{4}\right], \quad (\text{E5a})$$

$$\Delta N_\xi(\zeta, t) = \frac{2C}{t} \sqrt{\frac{\pi\psi}{1+\psi}} \exp\left(-\frac{\zeta^2}{4}\right), \quad (\text{E5b})$$

for all t . This completes the proof.

APPENDIX F: EFFECTIVE INTEGRAL OF DENSITY DISTURBANCES

In this Appendix, we calculate the effective integral over near zone, as discussed in Sect. VD2. If the trail density is the major contribution to the integral over the effective region then $\Delta N_{\zeta_1} \approx \Delta N_{\text{Trail}}(\xi)$, where $\Delta N_{\text{Trail}}(\xi) = \sqrt{\pi q_0/q(t)} (n_0 t_0/t) \exp[-\xi^2/4q(t)]$ and $q_0 = \psi/(1+\psi)$ [see Eqs. (C6) and (C9) in Appendix C]. If, however, we extend the integral over ζ to the entire half-axis $0 < \zeta < \infty$, then we will include the entire background plasma disturbances along this half-axis and obtain $\Delta N_\infty = \Delta N_\zeta/2(\xi) = \sqrt{\pi} (n_0 t_0/t) \exp(-\xi^2/4q_0)$, where ΔN_ζ is the density disturbance integral (DDI) over the entire ζ axis, Eq. (E5a). For $q(t) \simeq 1$, the difference between ΔN_{Trail} and ΔN_∞ is significant. The two integrals, however, are both Gaussian functions of ξ with peaks at $\xi = 0$. Their integrals over the entire ξ -axis, i.e., the 2D integrals of the trail density and the total density disturbances over the entire half-space $\zeta > 0$, are equal, $\int_{-\infty}^{\infty} \Delta N_{\text{Trail}} d\xi = \int_{-\infty}^{\infty} \Delta N_\infty d\xi = 2\pi\sqrt{q_0}(n_0 t_0/t)$. The true function $\Delta N_{\zeta_1}(\xi)$, taken over the effective region within the near zone, $0 < \zeta < \zeta_1$, should combine the entire contribution from the trail density with a part of the background density disturbances. It is natural to assume that $\Delta N_{\zeta_1}(\xi)$ varies between the two Gaussian functions, $\Delta N_{\text{Trail}}(\xi)$ and $\Delta N_\infty(\xi)$, and can be approximated by another Gaussian function with the peak at $\xi = 0$. This function should have the same integral over ξ , so that it is determined by one parameter \tilde{q} ,

$$\Delta N_{\zeta_1}(\xi) = \left(\frac{\pi q_0}{\tilde{q}}\right)^{1/2} \frac{n_0 t_0}{t} \exp\left(-\frac{\xi^2}{4\tilde{q}}\right). \quad (\text{F1})$$

The reason why the integral over ξ should be the same is that at any ζ beyond the trail the corresponding integral of the background density disturbances along ξ , Eq. (E5b), is exponentially small, as confirmed by our simulations.

The parameter $\tilde{q}(t)$ is similar to q in N_{Trail} and is uniquely related to the peak value $\Delta N_{\zeta_1}(0)$. From the derivation of Appendix C, it is clear that the adjusted parameter $\tilde{\rho}$ is related to \tilde{q} by the same relation as ρ to q , Eq. (25), i.e., $\tilde{\rho} = \gamma\tilde{q}t$. Thus to find $\tilde{\rho}$, we need to estimate $\Delta N_{\zeta_1}(0)$,

$$\Delta N_{\zeta_1}(0) = \left(\frac{\pi q_0}{\tilde{q}}\right)^{1/2} \frac{n_0 t_0}{t} = n_0 \left(\frac{\pi \rho_0 t_0}{\tilde{\rho} t}\right)^{1/2}. \quad (\text{F2})$$

The part of the corresponding integral stemming from the trail density is determined by q or by $\rho = \gamma qt$. To find the additional part stemming from the background density disturbances, we use Eq. (75), where we should replace ρ by $\tilde{\rho}$ because these disturbances are determined by the residual potential. While the constant value of $\delta n = 1/(1+\psi)\tilde{\rho}$ is easy to integrate, it is not so easy to determine the upper limit of integration, i.e., the exact value of ζ_1 .

It is clear, however, that ζ_1 should lie within the near zone, Eq. (20), so that $\zeta_1 = \beta/\alpha$, where $\alpha = (1+\psi)^{1/2}\Theta_0$, Eq. (B2), determines the typical scale ($\sim \alpha^{-1}$) of the residual potential variation along ζ and β is a numerical factor of order unity or less. Adding the two contributions and using Eq. (F2), we obtain

$$n_0 \left(\frac{\pi t_0 \rho_0}{t \tilde{\rho}}\right)^{1/2} = n_0 \left(\frac{\pi t_0 \rho_0}{t \rho}\right)^{1/2} + \frac{\beta}{2(1+\psi)^{3/2}\Theta_0 \tilde{\rho}}. \quad (\text{F3})$$

Manipulation with Eqs. (26) and (58) yields $2(1+\psi)^{3/2}\Theta_0 n_0 (t_0 \rho_0)^{1/2} = (1+\psi)/\gamma^{1/2}$, so that we can recast Eq. (F3) as a quadratic equation for $\sqrt{\tilde{\rho}/\rho}$,

$$\frac{\tilde{\rho}}{\rho} - \sqrt{\frac{\tilde{\rho}}{\rho}} + \frac{\tilde{\beta}}{2} = 0, \quad (\text{F4})$$

where

$$\tilde{\beta} = \frac{2\beta}{1+\psi} \sqrt{\frac{\gamma t}{\pi \rho}}. \quad (\text{F5})$$

Solving Eq. (F4), we obtain

$$\tilde{\rho}(t) = \frac{\rho(t)}{2} \left(1 - \tilde{\beta} \pm \sqrt{1 - 2\tilde{\beta}}\right). \quad (\text{F6})$$

Equation (F6) contains parameters β or $\tilde{\beta}$ which are still unknown functions of ρ and ψ . From Eq. (F6) it is clear that there exists an upper restriction on them ($\rho(t)/\gamma t \rightarrow 1$ as $\rho \rightarrow \infty$),

$$\tilde{\beta} \leq \tilde{\beta}_{\text{max}} = \frac{1}{2}, \quad \beta \leq \beta_{\text{max}} = \frac{\sqrt{\pi}(1+\psi)}{4}. \quad (\text{F7})$$

If we start from small values of ρ , as assumed by our theory, then we have to choose the solution with the ‘plus’ sign in front of the square root corresponding to $\tilde{\rho} \rightarrow \rho$ as $\tilde{\beta} \rightarrow 0$. In this case, the ratio $\tilde{\rho}/\rho$ decreases with increasing $\tilde{\beta}$, so that $\tilde{\rho}$ cannot be less than $\rho/4$. In our simulations, however, we found cases when, at least for some time, $\tilde{\rho}$ followed Eq. (F6) with the ‘minus’ sign in front of the square root, so that $\tilde{\rho}$ was less than $\rho/4$. These special cases ($\psi = 0.05$, $\Delta n_0 \lesssim 50$) usually start from sufficiently large values of ρ which are beyond the assumptions of our analytic theory.

While the strongest discrepancy between $\tilde{\rho}$ and ρ takes place for $\rho \gg 1$, the deviation between the two parameters starts developing at $\rho \sim 1$. Although the above heuristic derivation for $\tilde{\rho}$ is only valid for $\rho \gg 1$, we can formally extend Eqs. (F4)–(F6) to $\rho \sim 1$ and determine the function $\beta(\rho)$ numerically using comparison with simulations, see Sect. VII.

For $\psi \geq 0.05$, to good accuracy, the numerically found coupled functions $\beta(\rho)$ and $\tilde{\beta}(\rho)$ can be approximated by

$$\beta(\rho) \approx \frac{0.46\rho}{2.2 + \rho}, \quad \tilde{\beta}(\rho) \approx \frac{0.92\rho}{(1 + \psi)(2.2 + \rho)} \sqrt{\frac{\gamma t}{\pi\rho}}. \quad (\text{F8})$$

Note that for $\psi = 0.05$ at large time, $\tilde{\beta}$ asymptotically reached

the maximum value of $\tilde{\beta}_{\max} = 1/2$. We extrapolate this to smaller ψ keeping the same ρ -dependence as in Eq. (F8),

$$\beta(\rho) \approx \frac{\sqrt{\pi}(1 + \psi)\rho}{4(2.2 + \rho)}, \quad \tilde{\beta}(\rho) \approx \frac{\rho}{2(2.2 + \rho)} \sqrt{\frac{\gamma t}{\rho}}. \quad (\text{F9})$$

-
- [1] V. A. Bronshten, *Physics of Meteoric Phenomena* (Reidel Publishing Company, Dordrecht-Boston-Lancaster, 1983).
- [2] Z. Ceplecha, J. Borovicka, W. G. Elford, D. O. Revelle, R. L. Hawkes, V. Porubcan, and M. Simek, *Space Science Reviews* **84**, 327 (1998).
- [3] E. Chapin and E. Kudeki, *Geophys. Res. Lett.* **21**, 2433 (1994).
- [4] M. M. Oppenheim, A. F. vom Endt, and L. P. Dyrud, *Geophys. Res. Lett.* **27**, 3173 (2000).
- [5] S. Close, S. M. Hunt, M. J. Minardi, and F. M. McKeen, *Radio Science* **35**, 1233 (2000).
- [6] Q. H. Zhou, J. D. Mathews, and T. Nakamura, *Geophys. Res. Lett.* **28**, 1399 (2001).
- [7] M. M. Oppenheim, L. P. Dyrud, and L. Ray, *J. Geophys. Res.* **107**, submitted (2002).
- [8] L. P. Dyrud, M. M. Oppenheim, S. Close, and S. Hunt, *Geophys. Res. Lett.* **29**, CiteID 2012, DOI 10.1029/2002GL015953 (2002).
- [9] M. M. Oppenheim, A. F. vom Endt, and L. P. Dyrud, *Geophys. Res. Lett.* **27**, 3173 (2000).
- [10] L. P. Dyrud, M. M. Oppenheim, and A. F. vom Endt, *Geophys. Res. Lett.* **28**, 2775 (2001).
- [11] M. M. Oppenheim, L. P. Dyrud, and A. F. vom Endt, *J. Geophys. Res.* **108**, CiteID 1064, DOI 10.1029/2002JA009549 (2003).
- [12] L. P. Dyrud, L. Ray, M. Oppenheim, S. Close, and K. Denney, *J. Atmos. Solar-Terr. Phys.* **67**, 1171 (2005).
- [13] S. Close, M. M. Oppenheim, S. Hunt, and L. P. Dyrud, *J. Geophys. Res.* **107**, doi:10.1029/2002JA009253 (2002).
- [14] T. R. Kaiser, W. M. Pickering, and C. D. Watkins, *Planet. Space Sci.* **17**, 519 (1969).
- [15] W. M. Pickering and D. W. Windle, *Planet. Space Sci.* **18**, 1153 (1970).
- [16] A. M. Lyatskaya and M. P. Klimov, *J. Atmos. Terr. Phys.* **50**, 1007 (1988).
- [17] W. Jones, *Planet. Space Sci.* **39**, 1283 (1991).
- [18] R. E. Robson, *Phys. Rev. E* **63**, 026404 (2001).
- [19] W. G. Elford and M. T. Elford, in *ESA SP-495: Meteoroids 2001 Conference* (2001), pp. 357–359.
- [20] W. Jones, *Mon. Not R. Astron. Soc.* **275**, 812 (1995).
- [21] Y. S. Dimant and M. M. Oppenheim, *J. Atmos. Terr. Phys.* **66**, 1639 (2004).
- [22] R. Estrada and R. P. Kanwal, *Singular Integral Equations* (Birkhauser, Boston-Basel-Berlin, 2000).
- [23] N. I. Muskhelishvili, *Singular Integral Equations* (Wolters-Noordhoff, Groningen, Netherlands, 1972).
- [24] C. Price and M. Blum, *Earth, Moon, and Planets* (1998) **82/83**, 545 (2000).
- [25] R. Trautner, D. Koschny, O. Witasse, J. Zender, and A. Knöfel, in *ESA SP-500: Asteroids, Comets, and Meteors: ACM 2002* (2002), pp. 161–164.
- [26] D. T. Farley, *J. Geophys. Res.* **68**, 6083 (1963).
- [27] O. Buneman, *Phys. Rev. Lett.* **10**, 285 (1963).
- [28] D. T. Farley, *J. Atmos. Terr. Phys.* **47**, 729 (1985).
- [29] A. Papoulis, *The Fourier Integral and Its Applications* (McGraw-Hill, New York, 1987).
- [30] R. N. Bracewell, *The Fourier Transform and Its Applications* (McGraw-Hill, New York, 2000).
- [31] URL: www.pdesolutions.com
- [32] E. W. Weisstein, "Lambert W-Function," from *MathWorld-A Wolfram Web Resource*, <http://mathworld.wolfram.com/LambertW-Function.html>